DOT/FAA/AR-98/66

Office of Aviation Research
Washington, D.C. 20591

# Supplemental Inspection Document Development Program for the Cessna Model 402



March 1999

Final Report

This document is available to the U.S. public through the National Technical Information Service (NTIS), Springfield, Virginia 22161.

U.S. Department of Transportation
**Federal Aviation Administration**

## NOTICE

This document is disseminated under the sponsorship of the U.S. Department of Transportation in the interest of information exchange. The United States Government assumes no liability for the contents or use thereof. The United States Government does not endorse products or manufacturers. Trade or manufacturer's names appear herein solely because they are considered essential to the objective of this report. This document does not constitute FAA certification policy. Consult your local FAA aircraft certification office as to its use.

This report is available at the Federal Aviation Administration William J. Hughes Technical Center's Full-Text Technical Reports page: www.tc.faa.gov/its/act141/reportpage.html in Adobe Acrobat portable document format (PDF).

**Technical Report Documentation Page**

| 1. Report No. | 2. Government Accession No. | 3. Recipient's Catalog No. |
|---|---|---|
| DOT/FAA/AR-98/66 | | |

| 4. Title and Subtitle | 5. Report Date |
|---|---|
| SUPPLEMENTAL INSPECTION DOCUMENT DEVELOPMENT PROGRAM FOR THE CESSNA MODEL 402 | March 1999 |
| | 6. Performing Organization Code |
| 7. Author(s) | 8. Performing Organization Report No. |
| Larry Chan, Everett Foster, Beth Gamble, and Dan Townsend | |
| 9. Performing Organization Name and Address | 10. Work Unit No. (TRAIS) |
| Cessna Aircraft Company<br>1 Cessna Boulevard<br>Wichita, Kansas 67277 | 11. Contract or Grant No.<br>DTFA03-95-C-00044 |
| 12. Sponsoring Agency Name and Address | 13. Type of Report and Period Covered |
| U.S. Department of Transportation<br>Federal Aviation Administration<br>Office of Aviation Research<br>Washington, DC 20591 | Final Report, 10/95-4/98 |
| | 14. Sponsoring Agency Code<br>ACE-102 |

15. Supplementary Notes

Federal Aviation Administration William J. Hughes Technical Center COTR: Dr. Michael Basehore

16. Abstract

This document is the final report covering the results of a 2-year program. The program was funded through the Federal Aviation Administration (FAA) William J. Hughes Technical Center at Atlantic City International Airport under FAA contract number DTFA03-95-00044. The Cessna Model 402 was selected by the FAA due to the relatively high percentage of this aircraft in the regional airline fleet. The program focused on developing a supplementary inspection document (SID) for all variants of the Cessna Model 402 based on state-of-the-art damage tolerance analysis techniques.

The Cessna Model 402 was designed and certified prior to the advent of Federal Aviation Regulations which require the aircraft structure to be substantiated fail safe and/or meet certain damage tolerance requirements. Hence, there was minimal design data available to use with state-of-the-art analytical methods. Therefore, new development tests, service experience, and applications of current technology in the areas of loads, stress, fatigue, and fracture mechanics were used to identify and establish structural inspections and modifications necessary to maintain safety and to provide for continuing structural integrity and airworthiness. These items were done and the SID was developed in three phases.

Phase 1 of the SID development program consisted of three tasks: (1) Identification of the Principle Structural Elements (PSE), (2) Identification of the Critical Areas of the Principle Structural Elements, and (3) Development of a Stress Spectrum for Each Critical Area.

Phase 2 of the SID development program consisted of seven tasks: (1) Collect Material Property Data, (2) Establishment of Initial Flaw Sizes for Each Critical Location, (3) Determine Inspectable Flaw Sizes for Each Critical Location, (4) Perform Crack Growth Analysis for Each Critical Area, (5) Establish Supplemental Inspection Threshold for Each Critical Area, (6) Establish Repeat Inspection Interval for Each Critical Area, and (7) Determine the Onset of Widespread Fatigue Damage (WFD).

Phase 3 of the SID development program consisted of developing the supplemental inspection document for the Cessna Model 402 and to publish the SID as a final report.

| 17. Key Words | 18. Distribution Statement |
|---|---|
| Widespread fatigue damage, Supplemental inspection document, Fatigue crack growth, Cessna Model 402 | This document is available to the public through the National Technical Information Service (NTIS) Springfield, Virginia 22161. |

| 19. Security Classif. (of this report) | 20. Security Classif. (of this page) | 21. No. of Pages | 22. Price |
|---|---|---|---|
| Unclassified | Unclassified | 71 | |

TABLE OF CONTENTS

LIST OF FIGURES

LIST OF TABLES

# EXECUTIVE SUMMARY

This document is the final report covering the results of a 2-year program. The program was funded through the Federal Aviation Administration (FAA) William J. Hughes Technical Center at Atlantic City International Airport under FAA contract number DTFA03-95-00044. The Cessna Model 402 was selected by the FAA due to the relatively high percentage of this aircraft in the regional airline fleet. The program focused on developing a supplementary inspection document (SID) for all variants of the Cessna Model 402 based on state-of-the-art damage tolerance analysis techniques.

The Cessna Model 402 was designed and certified prior to the advent of Federal Aviation Regulations which require the aircraft structure to be substantiated fail safe and/or meet certain damage tolerance requirements. Hence, there was minimal design data available to use with state-of-the-art analytical methods. Therefore, new development tests, service experience, and applications of current technology in the areas of loads, stress, fatigue, and fracture mechanics were used to identify and establish structural inspections and modifications necessary to maintain safety and to provide for continuing structural integrity and airworthiness. These items were done and the SID was developed in three phases.

Phase 1 of the SID development program consisted of three tasks:

a. Identification of the Principle Structural Elements (PSE)
b. Identification of the Critical Areas of the Principle Structural Elements
c. Development of a Stress Spectrum for Each Critical Area

Phase 2 of the SID development program consisted of seven tasks:

a. Collect Material Property Data
b. Establishment of Initial Flaw Sizes for Each Critical Location
c. Determine Inspectable Flaw Sizes for Each Critical Location
d. Perform Crack Growth Analysis for Each Critical Area
e. Establish Supplemental Inspection Threshold for Each Critical Area
f. Establish Repeat Inspection Interval for Each Critical Area
g. Determine the Onset of Widespread Fatigue Damage

Phase 3 of the SID development program consisted of developing the supplemental inspection document for the Model 402 and publishing it as a final report (this report).

# 1. INTRODUCTION.

This document is the final report covering the results of a 2-year program. The program was funded through the Federal Aviation Administration (FAA) William J. Hughes Technical Center at Atlantic City International Airport under FAA contract number DTFA03-95-00044 [1]. The Cessna Model 402 was selected by the FAA due to the relatively high percentage of this aircraft in the regional airline fleet. The program focused on developing a supplementary inspection document (SID) for all variants of the Cessna Model 402 based on state-of-the-art damage tolerance analysis techniques.

## 1.1 PROGRAM OBJECTIVES.

The objective of this program was to perform a state-of-the-art damage tolerance analysis of the Cessna Model 402, a design which was certified prior to the advent of Federal Aviation Regulations (FAR) which required the aircraft structure to be substantiated fail safe and/or meet certain damage tolerance regulations. A SID was then developed based on the damage tolerance analysis, new and previously existing development test data, service experience, and teardown of high-time aircraft. The onset of widespread fatigue damage for the wing structure was also considered. The SID identifies and establishes structural inspections and modifications necessary to maintain safety and provide for continuing structural integrity and airworthiness. State-of-the-art nondestructive inspection techniques were evaluated and incorporated into the SID. Existing and new inspection requirements were evaluated with respect to suitability for widespread fatigue damage detection.

## 1.2 AIRCRAFT DESCRIPTION.

The Cessna Model 402, a twin engine piston airplane capable of seating up to nine passengers, was first produced in 1967. Three models which are structurally identical, the 402, 402A, and 402B, were produced. These models are equipped with tip tanks and have a dry wing. These airplanes will be referred to as the Model 402 through "B" throughout this report. Figure 1 presents a three-view drawing of the Model 402 through "B." In 1979, the Model 402C was introduced with a higher gross weight, a redesigned wet wing without tip tanks, and a redesigned vertical stabilizer. Figure 2 presents a three-view drawing of the Model 402C. Both the Model 402 through "B" and the Model 402C airframes were addressed in the damage tolerance assessment.

Over 2000 Model 402, 402A, 402B, and 402C airplanes had been built when production was terminated in 1985. Approximately 150 of these aircraft are used in commuter and sightseeing operations. The high-time aircraft has over twenty thousand flight hours.

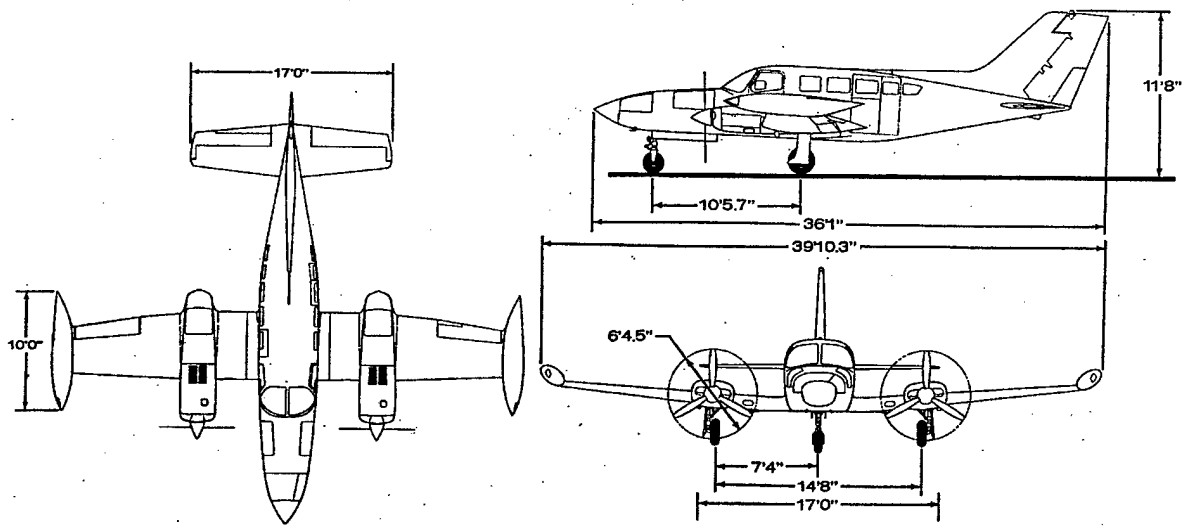


FIGURE 1. MODEL 402 THROUGH "B"

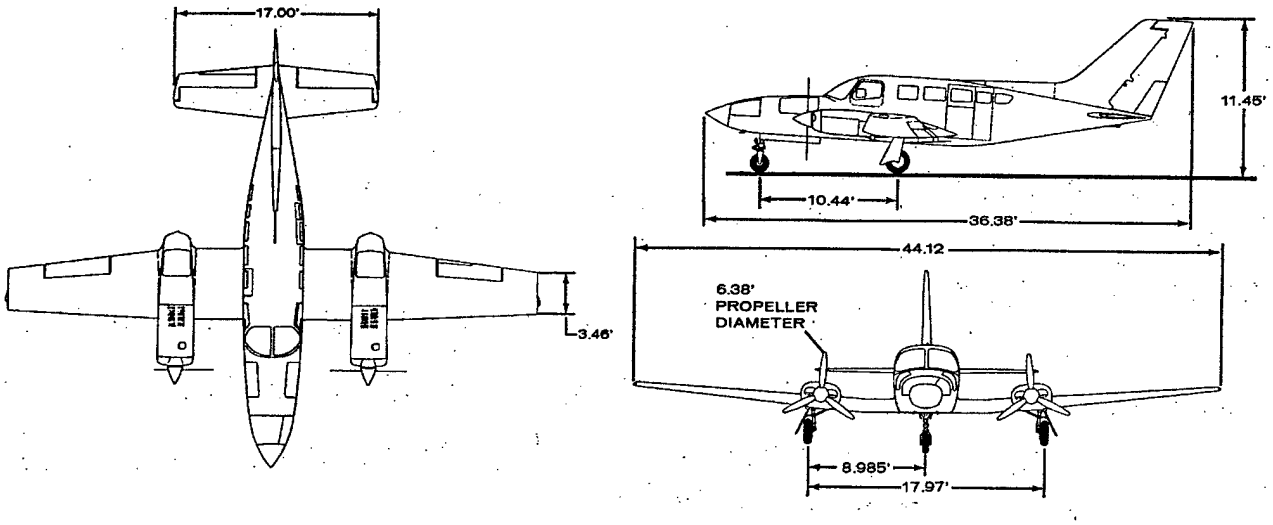


FIGURE 2. MODEL 402C

## 2. PHASE 1 TASKS.

### 2.1 IDENTIFICATION OF THE PRINCIPAL STRUCTURAL ELEMENTS (PSE).

A review of the Model 402 through "B" and Model 402C airframes was conducted to identify the Principal Structural Elements (PSE) which were candidates for detailed assessment. A component is classified as a PSE if the component contributes significantly to carrying flight and ground loads, and failure of the component could result in catastrophic failure of the airframe.

In order to determine the principal structural elements, detailed geometry and material information was collected for each airframe component. Service experience data were collected by surveying current Model 402 owners, by reviewing Cessna service bulletins, and by reviewing the FAA Service Difficulty Records. Finite element models were developed for both the Model 402 through "B" and Model 402C airframes. New limit load static tests were conducted to provide finite element model verification data, and fatigue test results were reviewed. The finite element models, static and fatigue test results, and service experience data are discussed in the following section. The airframe components which were identified as PSE are listed in table 1.

TABLE 1. PRINCIPAL STRUCTURAL ELEMENTS

| Component | Structure |
|---|---|
| Wing | • wing and carry-thru spar caps and attach fittings<br>• flaps, ailerons, and hinge fittings<br>• main landing gear and attachments |
| Horizontal Stabilizer | • stabilizer spar caps<br>• spar attach fittings<br>• elevator and hinge fittings |
| Vertical Stabilizer | • vertical stabilizer spar caps<br>• spar attach fittings<br>• rudder and hinge fittings |
| Engine | • engine mounts and support structure |
| Fuselage | • window longerons<br>• upper and lower cabin/tailcone stringers<br>• nose landing gear |

## 2.2 IDENTIFICATION OF THE CRITICAL AREAS OF THE PRINCIPAL STRUCTURAL ELEMENTS.

Several criteria are used to select the critical areas of the PSE. A critical area of a PSE is one that will require specific action, such as special inspections or repairs/modifications, in order to maintain continued airworthiness. The factors which are used to determine the PSE critical areas include:

- High stress levels
- Fatigue test results
- Service experience
- Inspectability
- Susceptibility to corrosion
- Susceptibility to accidental damage or impact

The critical areas of the PSEs are identified in section 2.2.4, along with an explanation as to why the area is critical. The criteria which were considered in determining critical areas are discussed in more detail in the sections listed below.

| Section | Criteria |
|---|---|
| 2.2.1 - Finite Element Models | • High stress levels |
| 2.2.2 - Supporting Test Evidence | • Fatigue cracking |
| 2.2.3 - Service Experience | • Service experience |
| | • Fatigue cracking |
| | • Susceptibility to corrosion or accidental damage |
| | • Inspectability |

2.2.1 Finite Element Models.

Finite element models were developed for the Model 402 through "B" and the Model 402C airframe components to establish internal loads and stresses in the airframe components. Finite element models were developed for the following components:

| | |
|---|---|
| MODEL 402 through "B" | • Wing and Carry-Thru |
| | • Flap and Aileron |
| | • Engine Beam |
| | • Fuselage |
| | • Horizontal Stabilizer and Elevator |
| | • Vertical Stabilizer and Rudder |
| | • Nose and Main Landing Gears |
| MODEL 402C | • Wing and Carry-Thru |
| | • Engine Beam |
| | • Vertical Stabilizer and Rudder |

Due to the commonality of many components between the Model 402 through "B" and the Model 402C, only one finite element model was made for each of the following: flap, aileron, fuselage, horizontal stabilizer, elevator, and the nose and main landing gears.

The MacNeal Schwendler Corporation's Version 68 of the National Aeronautics and Space Administration (NASA) Structural Analysis program (NASTRAN) was used for the finite element solution. To verify the finite element model, test stresses from the strain data collected during the ground tests (reference section 2.2.2.1) are compared to the model stresses for the associated analytical (model) static test cases.

Figures 3 and 4 show the finite element mesh for the M402C wing/carry-thru and fuselage model. The model is shown as two figures for clarity. This model uses CBEAM elements to represent the stringers and spar caps and CQUAD4 and CTRIA3 elements to represent the skins and webs. The model was tuned using NASTRAN runs for the maximum positive wing-bending limit load case, which is a condition covering the positive load envelope plus maximum engine

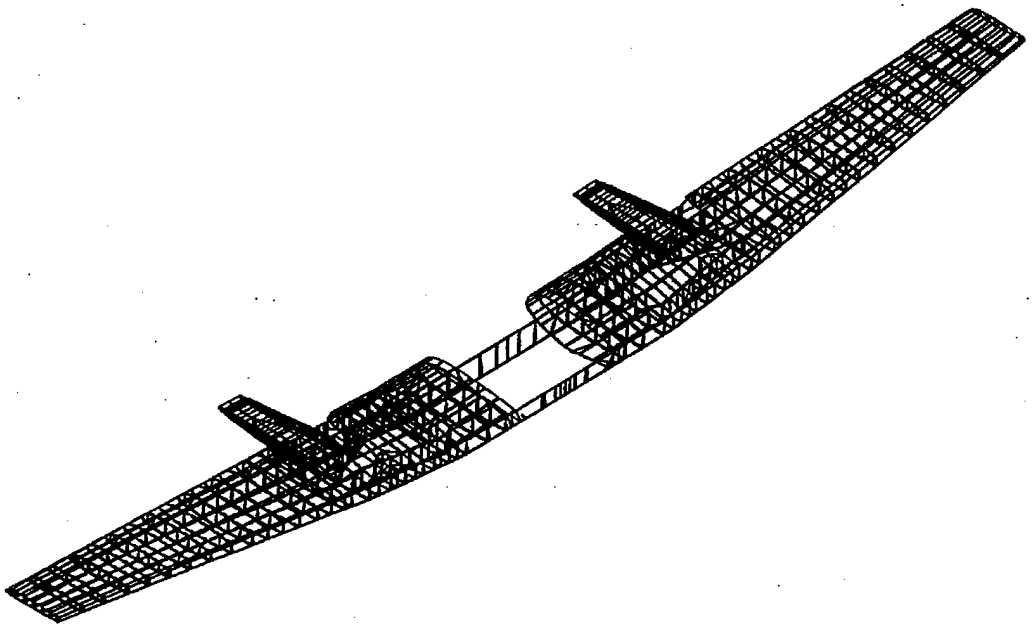

FIGURE 3. M402C WING AND CARRY-THRU FINITE ELEMENT MESH

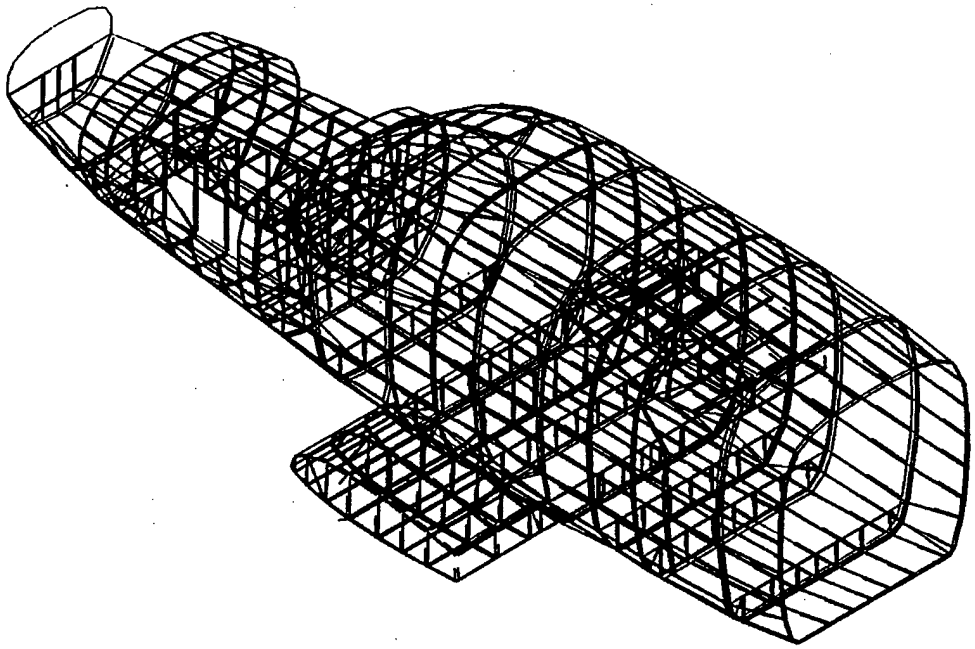

FIGURE 4. M402C FUSELAGE FINITE ELEMENT MESH

down load. The NASTRAN model was tuned to produce analytical stresses comparable to the test stresses upon applying the test loads to the model. The finite element mesh for the M402 through "B" wing/carry-thru and fuselage is very similar to the mesh produced for the M402C. This mesh is presented in section 3.1 of reference 2.

Figure 5 shows the finite element mesh of the M402C empennage. The model includes the tailcone, the vertical stabilizer, and the horizontal stabilizer. CBEAM elements are used to represent the stringers and spar caps and CSHEAR, CQUAD4, and CTRIA3 elements to represent the skins and the webs. Three load cases were determined to be critical after extensive analytical evaluation of the empennage structure. These three cases are rudder kick, maximum negative (down) maneuver, and maximum positive gust. The vertical stabilizer model was tuned using NASTRAN runs for the limit load condition of rudder kick. The horizontal stabilizer model was tuned using NASTRAN runs for the limit load conditions of maximum negative maneuver and maximum positive gust. The tailcone model was tuned using NASTRAN runs for all three limit load conditions. The NASTRAN runs were tuned to produce analytical stresses comparable to the test stresses upon applying the test loads to the model. The finite element mesh for the M402B empennage is very similar to the mesh of the M402C empennage. This mesh is presented in section 3.1 of reference 2.

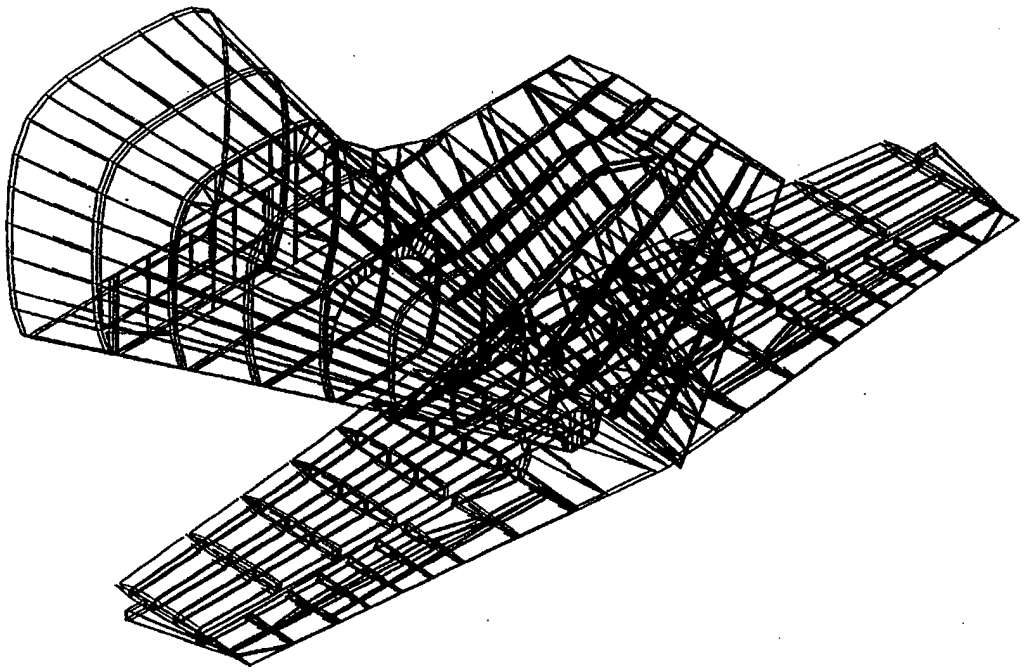

FIGURE 5. M402C EMPENNAGE FINITE ELEMENT MESH

Finite element meshes for the main and nose landing gear forgings are shown in figures 6 and 7. CTETRA elements are used to represent the gear forgings. CBEAM elements, which are not shown in the figures, are used to represent the main gear axle, barrel, torque link, and side brace actuator and the nose gear axle, barrel, torque link, and drag brace. Four limit load conditions were applied to each gear finite element model to determine the critical locations. Landing impact and ground handling conditions were considered.

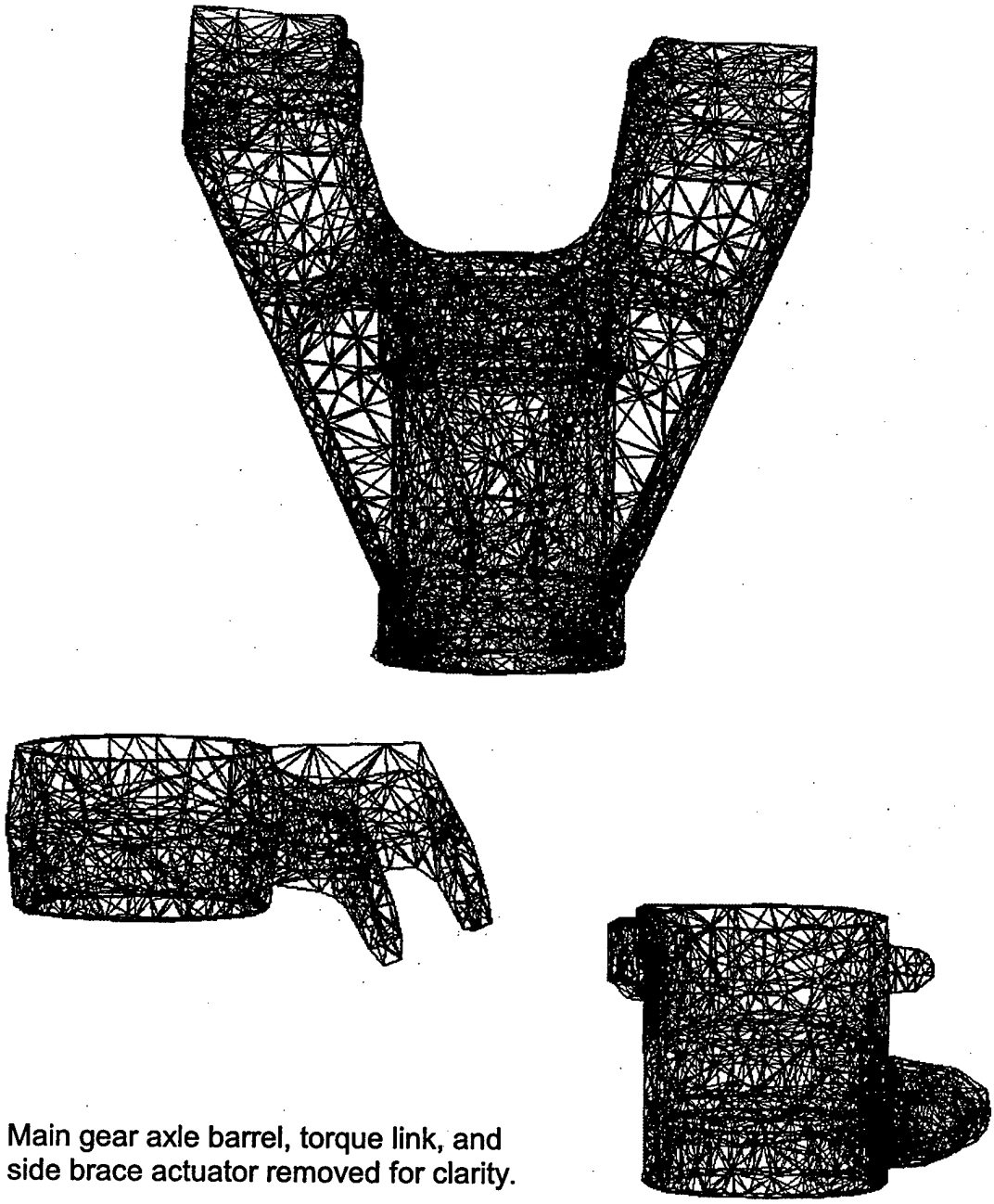


FIGURE 6. MAIN LANDING GEAR FINITE ELEMENT MESH

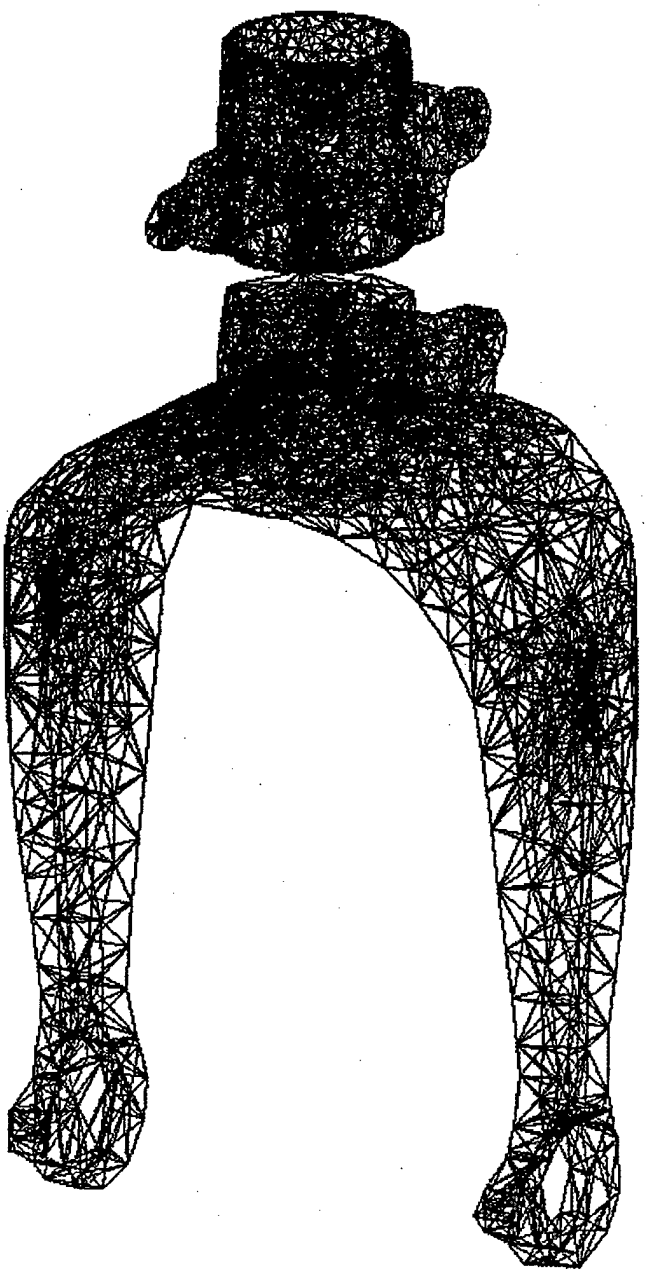

FIGURE 7. NOSE LANDING GEAR FORK FINITE ELEMENT MESH

2.2.2 Supporting Test Evidence.

2.2.2.1 Static Tests.

A series of limit load ground tests to provide finite element model verification data were conducted on a Model 402C wing. The wing ground test was conducted by attaching a left-hand wing, obtained from a salvage yard, to a Model 425 fuselage. A Model 402C right-hand wing was obtained to use as a loading fixture. One test, maximum positive wing bending, was conducted. This test condition covers the positive load envelope. The load envelope is a

composite of the flight critical loads, based on the requirements of Civil Air Regulation (CAR) conditions 3.183 through 3.190. A positive net (limit) load of 9470 lb. per wing plus a 3182 lb. negative load per engine was applied to each wing. Strain gauge and deflection data were recorded.

A series of limit load ground tests were also conducted on the Model 402C empennage. The tests were conducted on an empennage (tailcone and horizontal and vertical stabilizers) obtained from a salvage yard. Three load conditions were tested. These load conditions were selected based on extensive analytical evaluation of the empennage structure. The first load condition tested was the maximum negative (down) maneuver condition. A total limit down load of 1946 lb. was applied to the horizontal tail and elevators. The second load condition tested was the maximum positive gust load condition. The condition was tested to 94% of the total limit up load of 2658 lb. on the horizontal tail and elevators. The third load condition tested was the rudder kick condition. A total limit load of 1726 lb. was applied to the vertical tail and rudder. Strain gauge and deflection data were recorded. The stresses measured during both the wing and empennage tests were compared to the analytical stresses predicted by the finite element models. These comparisons were used to refine the finite element models.

2.2.2.2 Fatigue Tests.

Two component fatigue tests have been completed in the past on Model 400 series wings. A single wing, block loaded, cyclic test was conducted on the Model 402 through "B" in the mid-1970s. This test was conducted to obtain fatigue data which would aid in the establishment of service lives for the Model 402. Five locations developed fatigue cracks during the course of the test.

A fatigue test similar to the Model 402B wing component fatigue test was conducted on a Model 421C. The Model 421C wing is similar to the Model 402C wing, but with smaller spar caps. Two natural cracks of 0.05 in. length were found in the wing front spar after 80,000 test hours.

A summary of the test results is presented in section 3.2 of reference 2. The results of these fatigue tests were used to help determine the susceptibility to fatigue damage of the principle structural elements.

2.2.3 Service Experience.

Service experience was used to determine which areas of the PSEs were susceptible to fatigue cracking, corrosion, and/or accidental damage. In order to determine the service problems which have been reported in the field, three sources of information were used:

a. Cessna service bulletins.
b. Operator surveys inquiring about structural problems and repairs.
c. FAA Service Difficulty Records.

A summary of the Cessna service bulletins is presented in section 3.3 of reference 2. The second method used to determine service experience problems was to review information supplied by

current operators. In conjunction with a survey sent to current Model 402 operators to determine the usage of their airplanes, the operators were asked if they had encountered any major structural problems with their airplanes. A copy of the survey form is presented in figure 8. A summary of the operators' responses can be found in section 3.2 of reference 2.

INFORMATION NEEDED TO DEVELOP FATIGUE ANALYSIS

**This form should be filled out for each aircraft in the fleet. The specific information about each individual aircraft is important in developing the history of usage of the aircraft fleet and the structural locations critical with service.**

| Aircraft Serial No. | | Model 402 A B C (circle) |
|---|---|---|
| Total Service Time Of Aircraft | | hrs. |
| Auxiliary Tank Locations (outb'd, wing locker, etc.) and Capacity Of Each | | |
| Aux. Tank # | Location | gals. |
| Aux. Tank # | Location | gals. |
| Aux. Tank # | Location | gals. |
| Aux. Tank # | Location | gals. |

| Structural Airframe Repairs (Optional) |
|---|
| Describe any significant structural repairs made to the aircraft and where these repairs are located. List the repairs which were required because of longevity of service, not those required routinely to meet airworthiness regulations. This information will be used by Cessna engineers to help determine which locations are to be included in the fatigue analysis. Continue on the back of the sheet if necessary. |
| |
| |
| |
| |
| |
| |
| |
| |
| |
| |
| |
| |
| |
| |
| |
| |
| |

FIGURE 8. OPERATOR SURVEY—AIRFRAME REPAIRS

The third method of determining structural problems which have occurred in the field was to review excerpts of the Service Difficulty records provided by the FAA. These records cover the period of time from the mid-1970s to December 1995. A summary of the problems which appeared more than once in these records is presented in section 3.3 of reference 2.

2.2.4 PSE Critical Areas.

Tables 2 and 3 present the PSE critical areas chosen for analysis. Figures 9 through 22 show the locations of these PSE critical areas.

TABLE 2. MODEL 402C ANALYSIS LOCATIONS

| ID | Figure Number | Description | Selection Criteria* |
|---|---|---|---|
| CW-1 | 10 | Wing Lower Carry-Thru Front Spar Cap, B.L. 48.00 | 1,2 |
| CW-2 | 9 | Wing Lower Front Spar Cap at Root Fitting Attach, W.S. 66.70 | 1,2 |
| CW-3 | 9 | Wing Lower Front Spar Cap at Canted Rib Attachment, W.S. 80.52 | 1 |
| CW-4 | 9 | Wing Lower Front Spar Cap at Inboard Engine Beam Attach, W.S. 88.05 | 1 |
| CW-5 | 9 | Wing Lower Front Spar at Outboard Engine Beam Attach, W.S. 107.02 | 1,2 |
| CW-6 | 9 | Wing Lower Front Spar Cap at Skin Splice, W.S. 119.74 | 1,3 |
| CW-7 | 9 | Wing Lower Forward Auxiliary Spar Cap, W.S. 81.20 | 1 |
| CW-8 | 9 | Wing Lower Aft Auxiliary Spar Cap, W.S. 96.64 | 1 |
| CW-9 | 9 | Wing Rear Spar Lower Cap at Splice, W.S. 110.24 | 1 |
| CW-10 | 10 | Wing Lower Carry-Thru Rear Spar Cap, B.L. 49.50 | 1,3 |
| CW-11 | 9 | Wing Upper Front Spar Cap, W.S. 108.008 | 1,3 |
| CEB-1 | 9 | Engine Beam at Aft Engine Mount, F.S. 127.15 | 1,3 |
| CF-1 | 11 | Fuselage Left Hand Longeron, F.S. 190.33 | 1 |
| CF-2 | 11 | Tailcone Angle Attachment to Horizontal Rear Spar, B.L. 2.90 | 1 |
| CH-1 | 12 | Horizontal Stabilizer Forward Spar Upper Cap, B.L. 0.0 | 1 |
| CH-2 | 12 | Horizontal Stabilizer Forward Spar Lower Cap, B.L. 0.0 | 1 |
| CH-3 | 12 | Horizontal Stabilizer Forward Spar Attach Bolt through Web, B.L. 7.69 | 1,3 |
| CH-4 | 12 | Horizontal Stabilizer Rear Spar Lower Cap at Attach Bolt, B.L. 2.90 | 1 |
| CH-5 | 12 | Horizontal Stabilizer Rear Spar Upper Cap, B.L. 0.0 | 1 |
| CH-6 | 12 | Horizontal Stabilizer Rear Spar Lower Cap, B.L. 0.0 | 1 |
| CH-7 | 12 | Horizontal Stabilizer Rear Auxiliary Spar Upper Cap, B.L. 8.01 | 1 |
| CV-1 | 13 | Vertical Stabilizer Rear Spar at Attachment, W.L. 108.38 | 1 |
| CV-2 | 13 | Vertical Stabilizer Rear Spar Cap at W.L. 136.04 | 1 |
| CMLG-1 | 14 | Main Landing Gear Side Brace Actuator Collar | 1,3 |
| CNLG-1 | 15 | Nose Landing Gear Fork | 1,3 |

* Selection Criteria:
1. High stress levels from finite element model
2. Fatigue test results
3. Service experience

TABLE 3. MODEL 402 THROUGH "B" ANALYSIS LOCATIONS

| ID | Figure Number | Description | Selection Criteria* |
|---|---|---|---|
| BW-1 | 17 | Wing Lower Carry-Thru Front Spar Cap, B.L. 36.12 | 1,2 |
| BW-2 | 16 | Wing Lower Front Spar Cap Root Fitting, W.S. 46.70 | 1,2,3 |
| BW-3 | 16 | Wing Lower Front Spar Cap Root Fitting Attach, W.S. 54.10 | 1,2,3 |
| BW-4 | 16 | Wing Lower Front Spar Cap Canted Rib Attachment, W.S. 66.70 | 1,2 |
| BW-5 | 16 | Wing Lower Front Spar Cap, W.S. 75.66 | 1,3 |
| BW-6 | 16 | Wing Lower Front Spar Cap at Inboard Engine Beam Attach, W.S. 83.74 | 1,3 |
| BW-7 | 16 | Wing Lower Front Spar Cap at Outboard Engine Beam Attach, W.S. 98.74 | 1,3 |
| BW-8 | 16 | Wing Lower Forward Auxiliary Spar Cap at W.S. 86.62 | 1 |
| BW-9 | 16 | Wing Lower Aft Auxiliary Spar Cap at W.S. 89.65 | 1 |
| BW-10 | 17 | Wing Lower Carry-Thru Rear Spar Cap, B.L. 37.60 | 1 |
| BW-11 | 16 | Wing Rear Spar Cap at Splice, W.S. 98.14 | 1 |
| BW-12 | 16 | Wing Upper Front Spar Cap, W.S. 106.82 | 1,3 |
| BEB-1 | 16 | Engine Beam at Aft Engine Mount, F.S. 131.20 | 1,3 |
| BF-1 | 18 | Fuselage Left Hand Longeron, F.S. 190.33 | 1 |
| BF-2 | 18 | Tailcone Angle Attachment to Horizontal Rear Spar, B.L. 2.90 | 1 |
| BH-1 | 19 | Horizontal Stabilizer Forward Spar Upper Cap, B.L. 0.0 | 1 |
| BH-2 | 19 | Horizontal Stabilizer Forward Spar Lower Cap, B.L. 0.0 | 1 |
| BH-3 | 19 | Horizontal Stabilizer Forward Spar Attach Bolt Through Web, B.L. 7.69 | 1,3 |
| BH-4 | 19 | Horizontal Stabilizer Rear Spar Lower Cap at Attach Bolt, B.L. 2.90 | 1 |
| BH-5 | 19 | Horizontal Stabilizer Rear Spar Upper Cap, B.L. 0.0 | 1 |
| BH-6 | 19 | Horizontal Stabilizer Rear Spar Lower Cap, B.L. 0.0 | 1 |
| BH-7 | 19 | Horizontal Stabilizer Rear Auxiliary Spar Upper Cap, B.L. 8.01 | 1 |
| BV-1 | 20 | Vertical Stabilizer Rear Spar at Attachment, W.L. 108.38 | 1 |
| BV-2 | 20 | Vertical Stabilizer Rear Spar Cap, W.L. 136.04 | 1 |
| BMLG-1 | 21 | Main Landing Gear Side Brace Actuator Collar | 1,3 |
| BNLG-1 | 22 | Nose Landing Gear Fork | 1,3 |

* Selection Criteria:
1. High stress levels from finite element model
2. Fatigue test results
3. Service experience

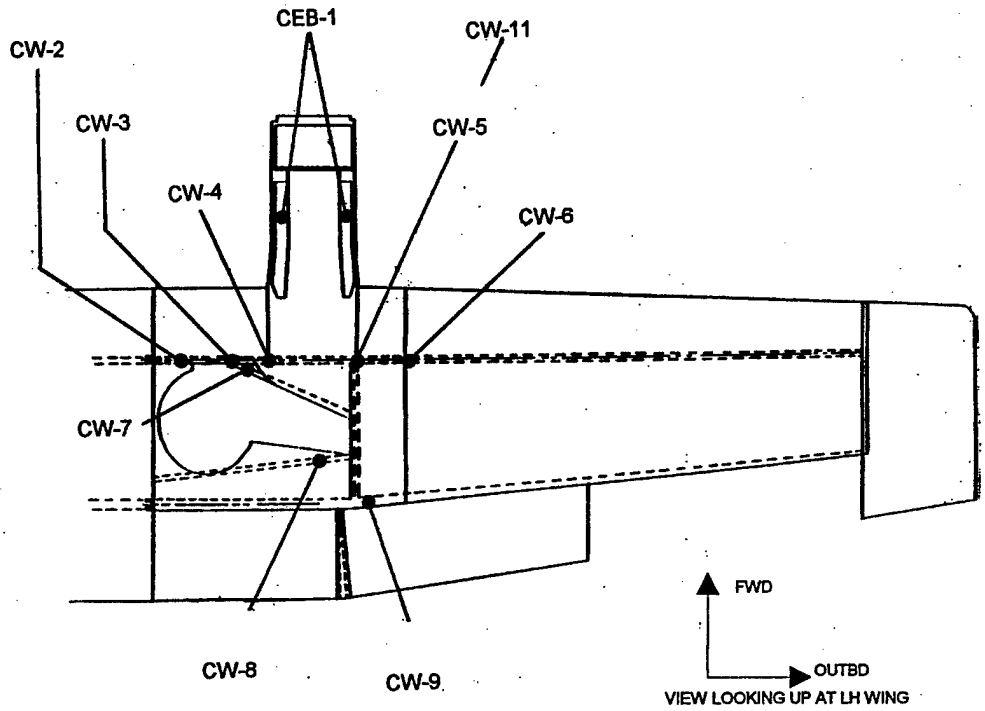


FIGURE 9. MODEL 402C WING ANALYSIS LOCATIONS

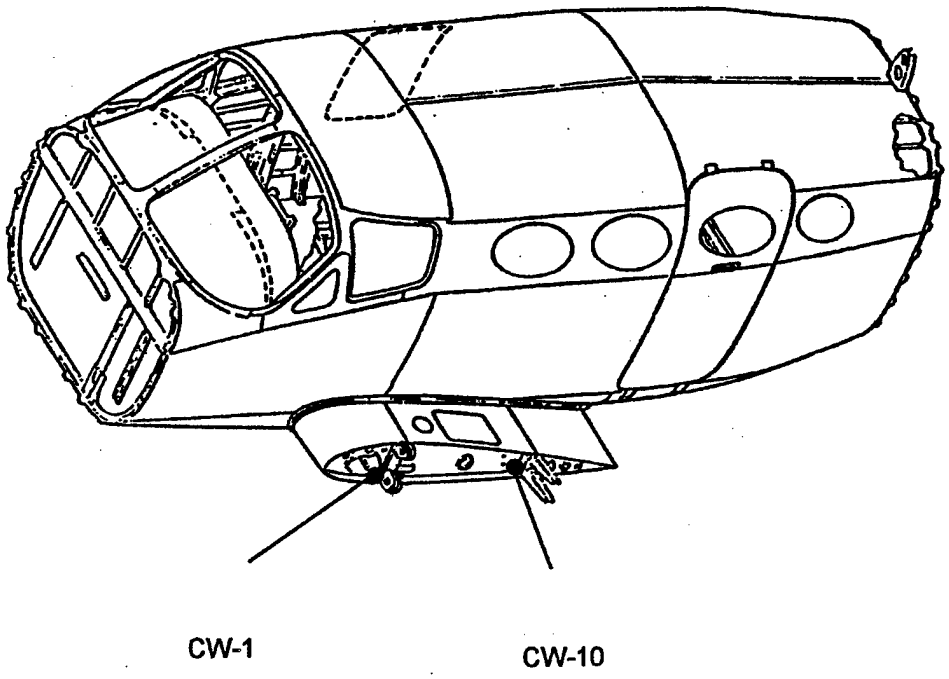


FIGURE 10. MODEL 402C STUB WING ANALYSIS LOCATIONS

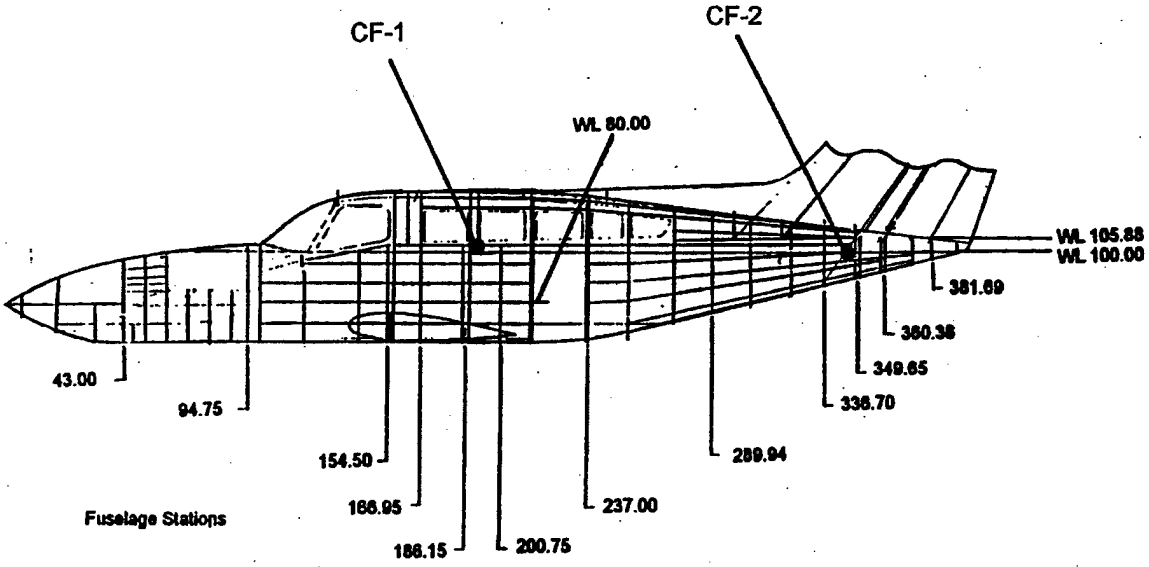


FIGURE 11. MODEL 402C FUSELAGE ANALYSIS LOCATIONS

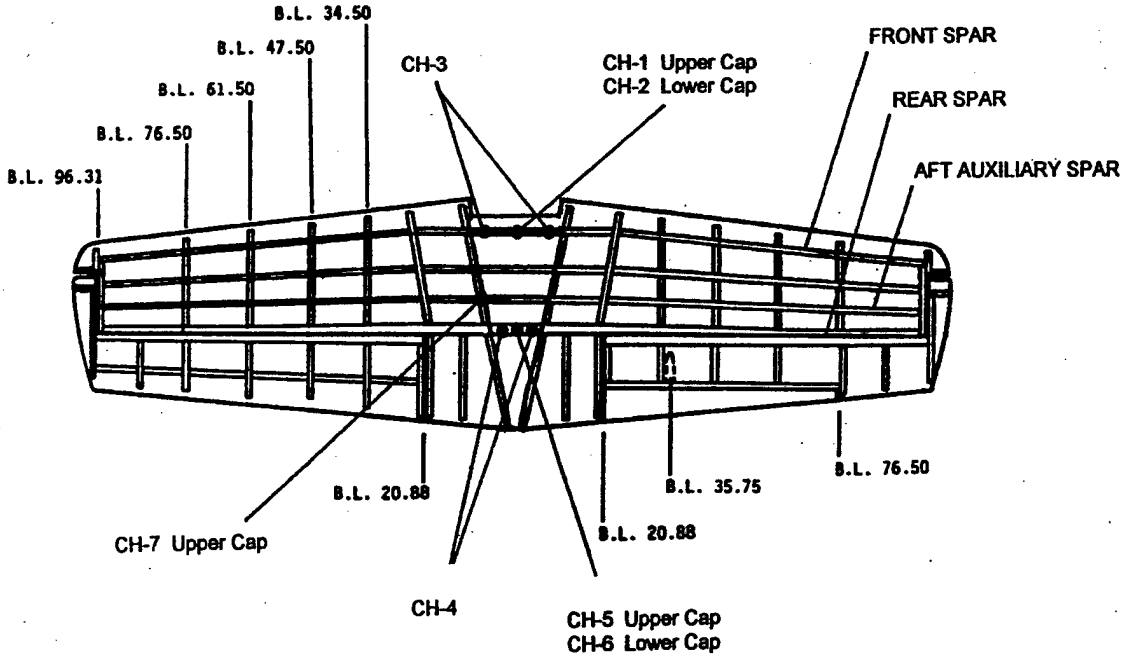


FIGURE 12. MODEL 402C HORIZONTAL STABILIZER ANALYSIS LOCATIONS

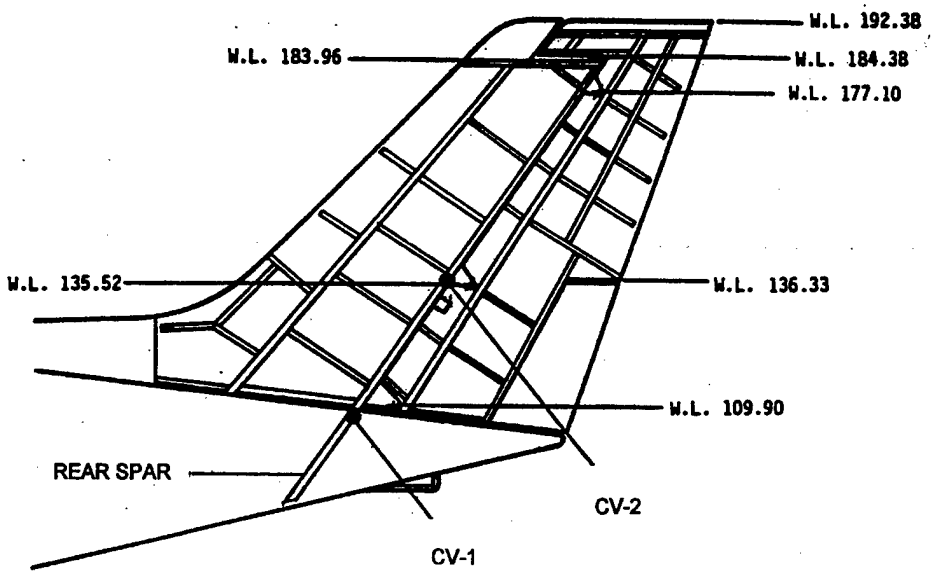


FIGURE 13. MODEL 402C VERTICAL STABILIZER ANALYSIS LOCATIONS

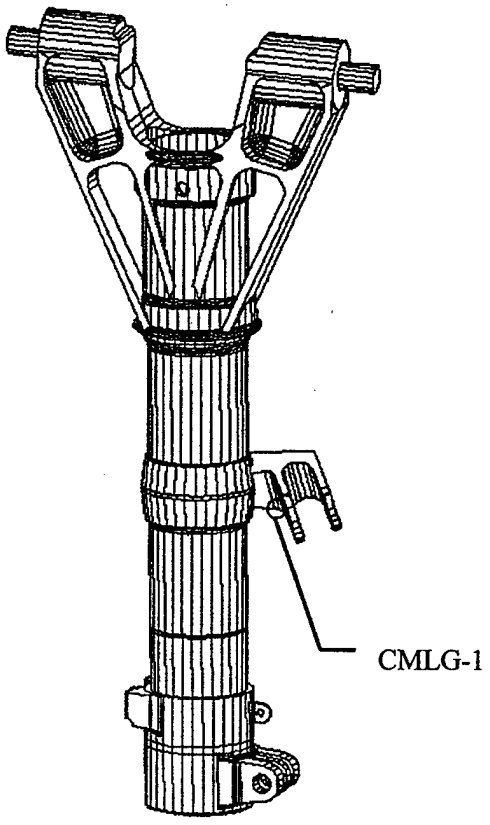


FIGURE 14. MODEL 402C MAIN LANDING GEAR SIDE BRACE ACTUATOR COLLAR ANALYSIS LOCATION

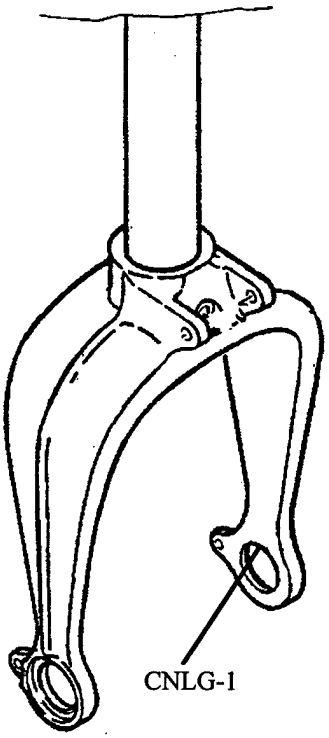


FIGURE 15. MODEL 402C NOSE LANDING GEAR FORK ANALYSIS LOCATION

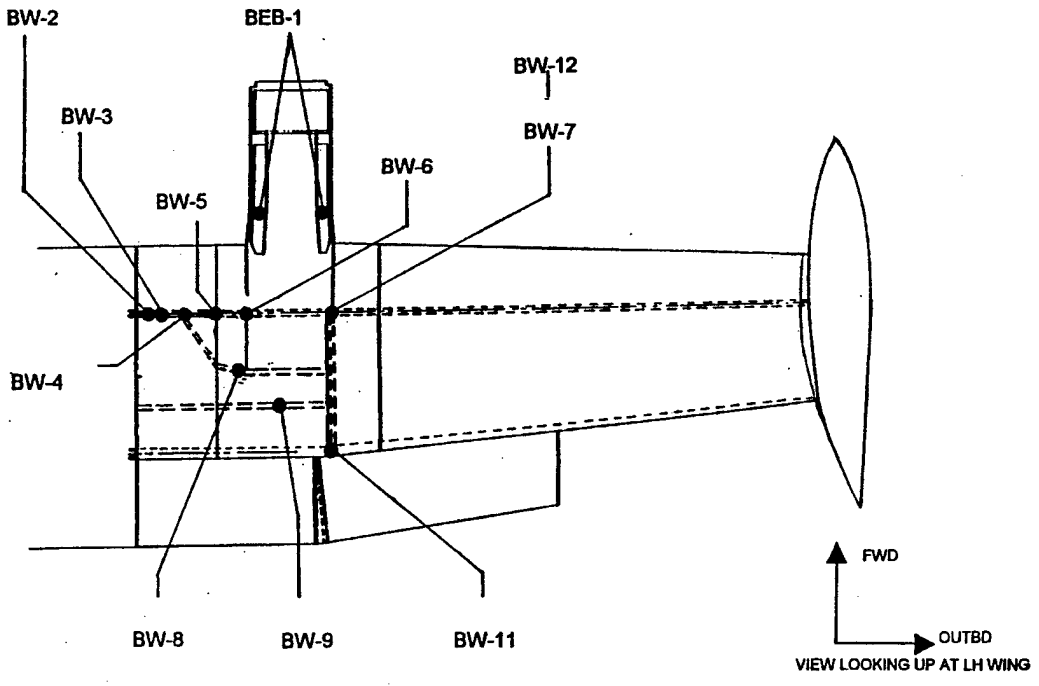


FIGURE 16. MODEL 402 THROUGH "B" WING ANALYSIS LOCATIONS

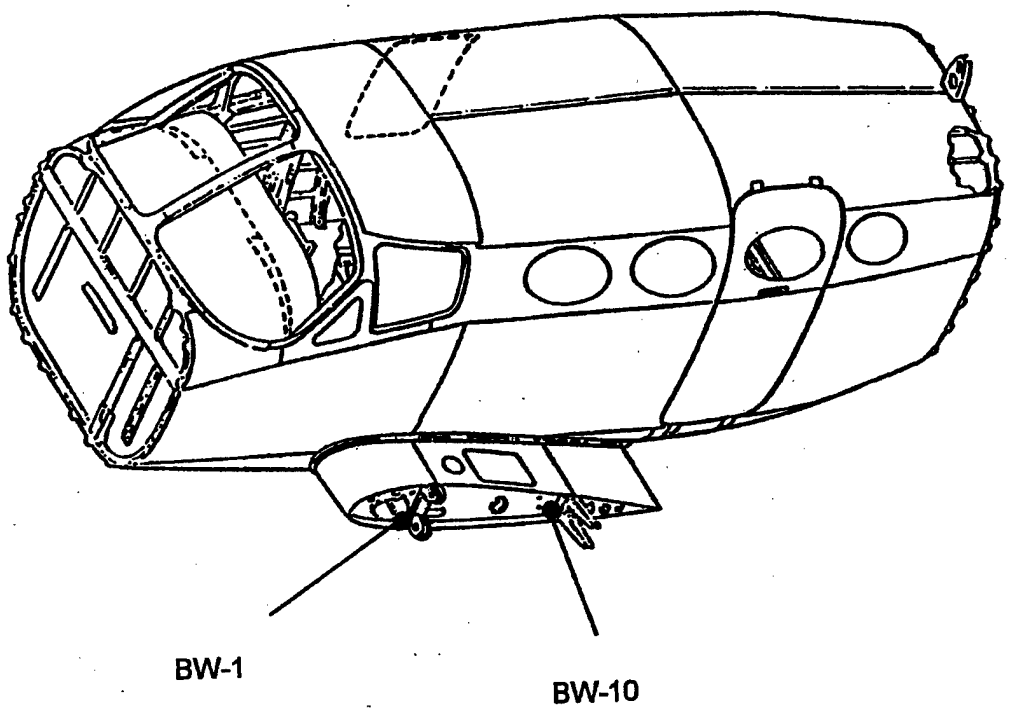


FIGURE 17. MODEL 402 THROUGH "B" STUB WING ANALYSIS LOCATIONS

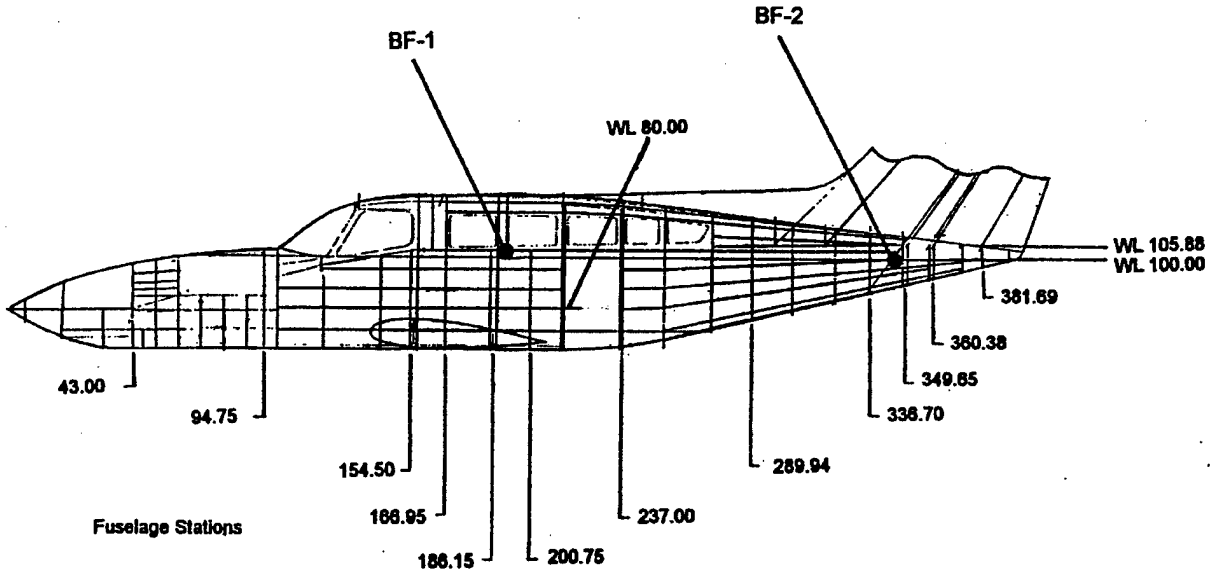


FIGURE 18. MODEL 402 THROUGH "B" FUSELAGE ANALYSIS LOCATIONS

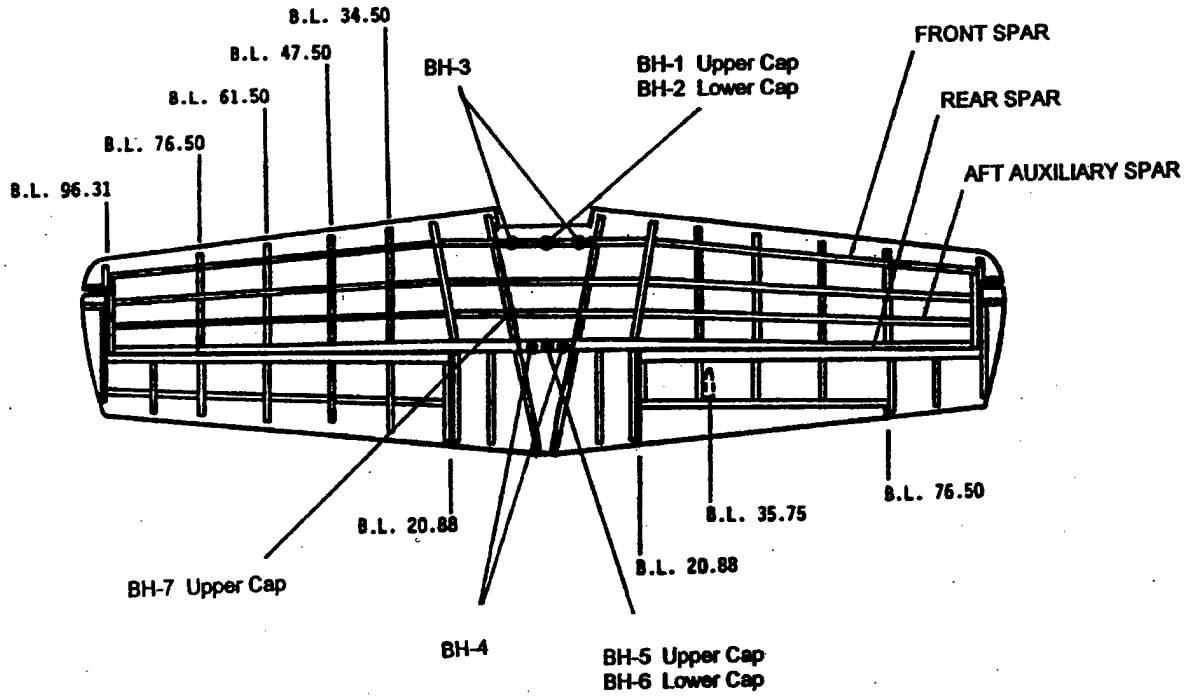


FIGURE 19. MODEL 402 THROUGH "B" HORIZONTAL STABILIZER ANALYSIS LOCATIONS

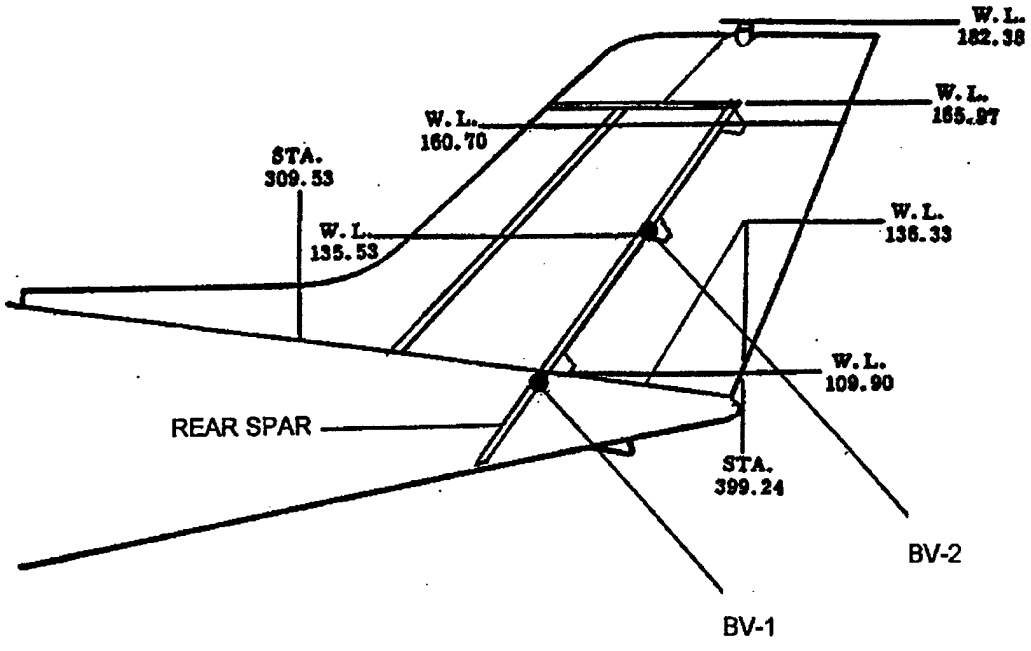


FIGURE 20. MODEL 402 THROUGH "B" VERTICAL STABILIZER ANALYSIS LOCATIONS

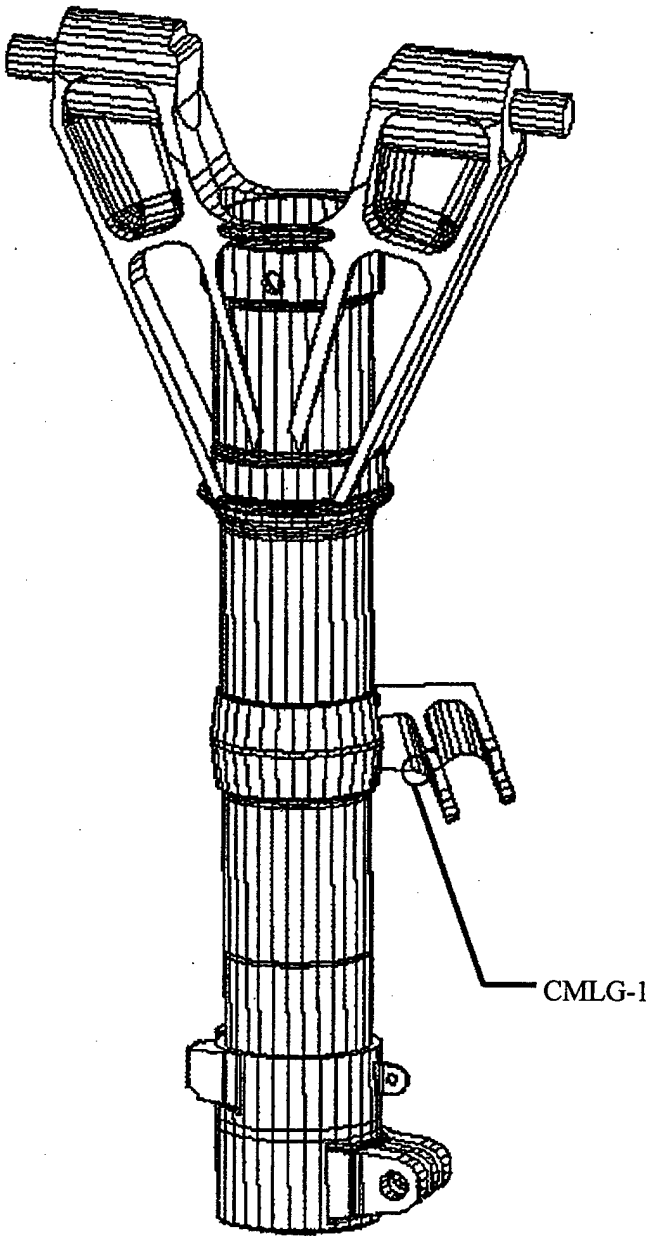


FIGURE 21. MODEL 402 THROUGH "B" MAIN LANDING GEAR SIDE BRACE ACTUATOR COLLAR ANALYSIS LOCATION

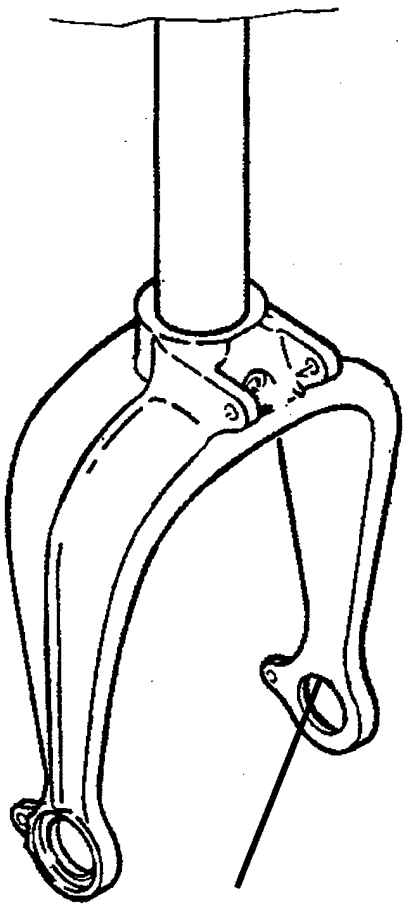

CNLG-1

FIGURE 22. MODEL 402 THROUGH "B" NOSE LANDING GEAR FORK ANALYSIS LOCATION

## 2.3 DEVELOPMENT OF A STRESS SPECTRUM FOR EACH CRITICAL AREA.

### 2.3.1 Operational Statistics of the Fleet.

The first step in developing the stress spectra was to determine how Model 402 commuter operators were using their aircraft. To accomplish this, a survey was developed and mailed to operators identified by the FAA. A copy of the survey form is shown in figure 23. The FAA identified 34 operators with 150 airplanes being used to carry either passengers or cargo. A total of 14 operators representing 85 airplanes returned the survey. This usage data was supplemented by a survey of three operators representing four airplanes conducted by Cessna in 1974. The airplanes included in the two surveys represent a usage of 2011 flights per week. The usage is shown in figure 24 and is represented by a three-parameter Weibull distribution shown in figure 25. After reviewing the data and the way in which the airplanes were flown by specific operators, three sets of mission profiles were developed. The profiles are discussed in section 2.3.2. This data was used to create the typical mission profiles used in the damage tolerance analysis.

INFORMATION NEEDED TO DEVELOP FLIGHT PROFILES FOR FATIGUE ANALYSIS

This form should be filled out to accurately describe a **typical** flight[1]. Weights, distribution of fuel, altitude above ground or water, speeds, and length of flight all have an effect on the fatigue life expected. The accuracy of the fatigue analysis depends on the accuracy of your information. If the typical flight changes, the individual fatigue analysis no longer would apply.

| | | | | |
|---|---|---|---|---|
| Aircraft Model 402 A B C (circle one) | | | | |
| Number of Times Typical Flight is Flown _____/week/month/year (circle one) | | | | |
| Percent Of Total Flight Time This Typical Flight Represents | | | | % |
| Airport Elevation (ft) | Takeoff - | | Landing - | |
| Ramp Weight[2] | | | | lbs |
| Takeoff Fuel Loading[3] | Main Tanks | | | lbs |
| | Aux. Tanks | | | lbs |
| | | | | lbs |
| | | | | lbs |
| Occupants and Baggage[4] | | | | lbs |
| Landing Weight[5] | | | | lbs |
| Landing Fuel Loading[3] | Main Tanks | | | lbs |
| | Aux. Tanks | | | lbs |
| | | | | lbs |
| | | | | lbs |
| Cruise Speed and Altitude | | KIAS | | ft |
| Terrain flown over and elevation[6] | land % water % | | | ft |
| Climb Speeds and Time[7] | grd -- | ft | KIAS | min |
| | | ft | KIAS | min |
| | | ft | KIAS | min |
| Descent Speeds and Time[7] | | ft | KIAS | min |
| | | ft | KIAS | min |
| | | -- grd ft | KIAS | min |
| Flight Length (hours or minutes) | | | | |

[1] Complete this form for each frequently flown flight profile (significantly different flight pattern).
[2] This is the total weight of the fueled aircraft, including crew and passengers and any baggage or cargo.
[3] This is the total weight of the fuel onboard, with the distribution noted if there are auxiliary tanks used.
[4] This is the total weight of the crew, passengers, and baggage or cargo.
[5] This is the weight at which this aircraft lands.
[6] If the terrain flown over is fairly flat, an average elevation may be used. If flying over varied elevations (i.e. - mountains and valleys) the flight path may be marked on an aeronautical chart that shows terrain elevation and submitted with this form.
[7] If altitude is over 7,000 ft. break down in 5,000 ft or less increments.

FIGURE 23. OPERATOR SURVEY—FLIGHT DATA

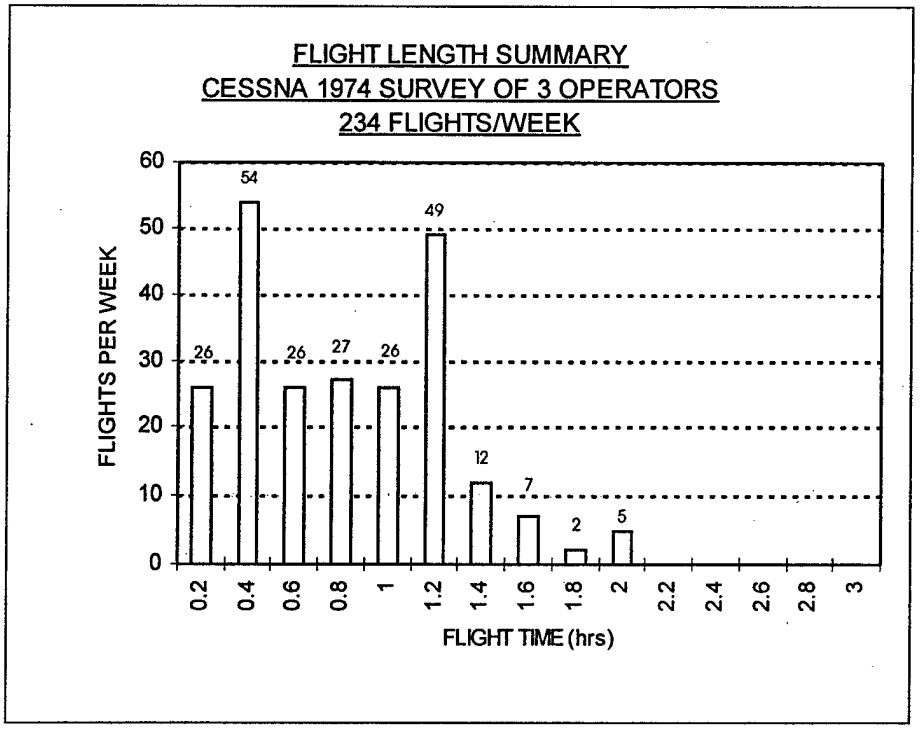


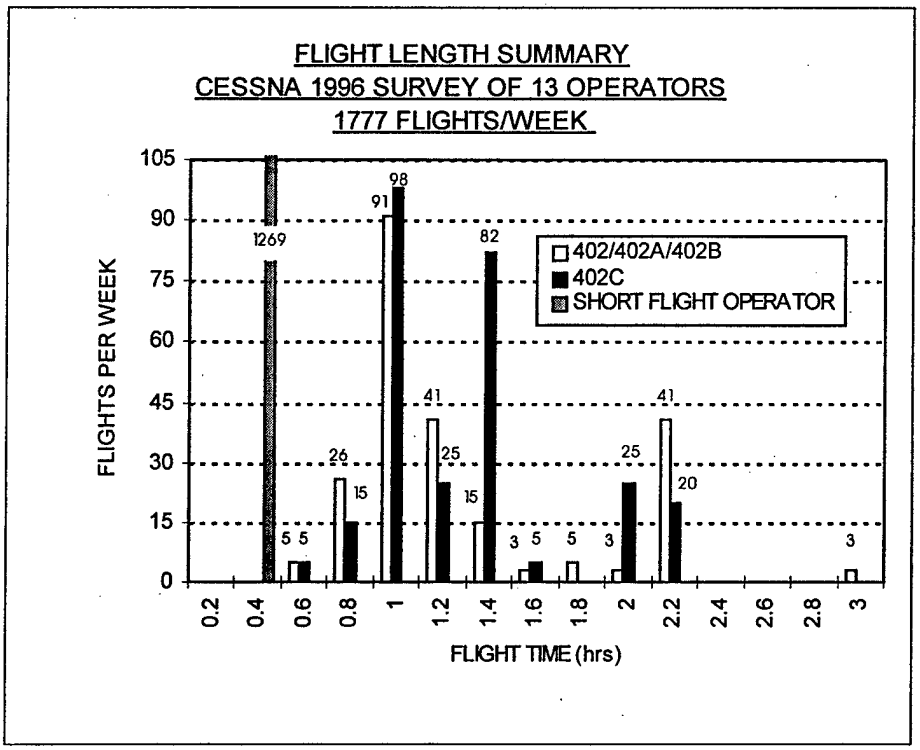


FIGURE 24. FLIGHT LENGTH SURVEY SUMMARIES

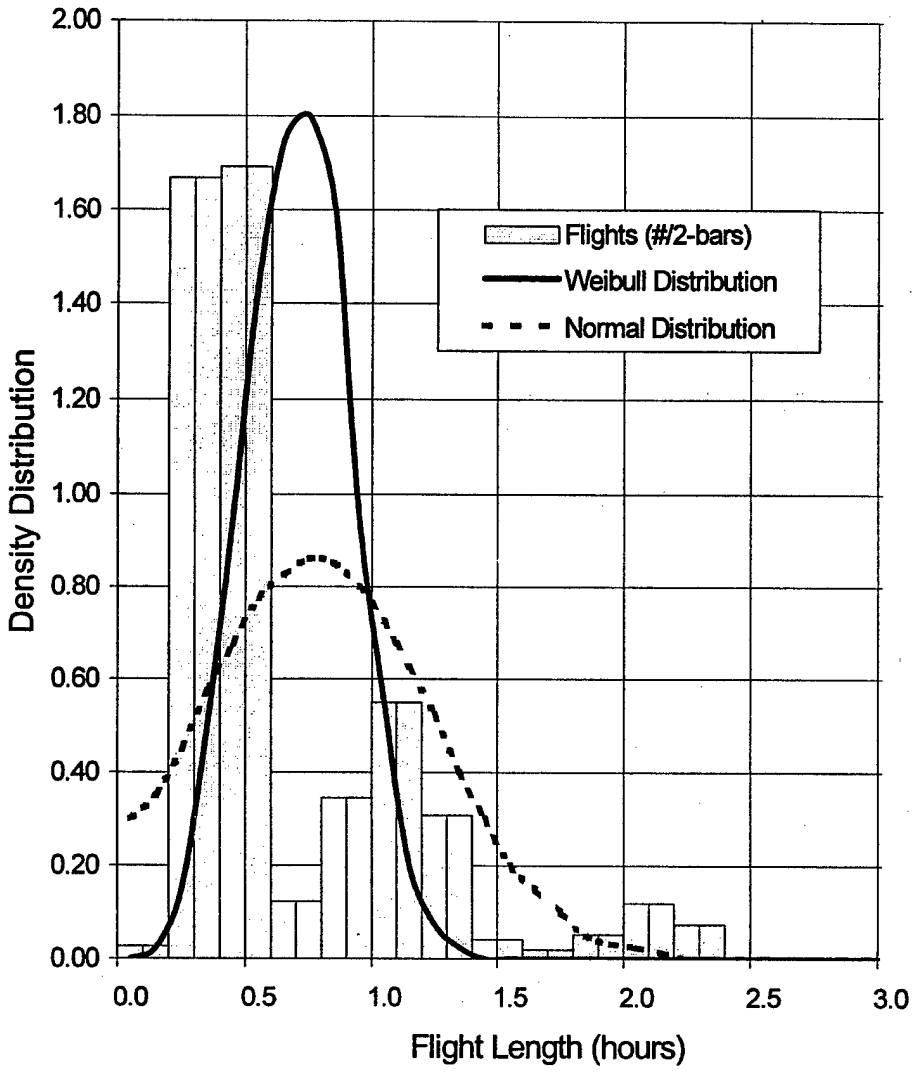


FIGURE 25. MODEL 402 FLIGHT LENGTH DISTRIBUTION—17 OPERATORS

2.3.2 Flight Profiles.

The flight profiles for the Model 402 were derived from the flight data reported by Model 402 operators in two surveys conducted in 1974 and 1996. The data collected includes takeoff fuel weights, takeoff gross weights, passenger loading, flight altitudes, and flight lengths. After reviewing the flight data and specific mission profiles flown by operators, three sets of profiles were developed for use in fatigue and crack growth analysis.

The first profile set is called the Short Flight Profile and consists of one flight profile. This flight profile was developed to represent operators who use their airplanes only for short missions of about 25 minutes in length. The Short Flight Profile was used for analysis of Model 402C aircraft only. Table 4 presents details of the Short Flight Profile.

TABLE 4. FLIGHT PROFILE DEFINITIONS SHORT FLIGHT—MODEL 402C

| Flight Profile Number | Number of Persons Onboard | Ramp Weight (Lbs) | Ramp Fuel (Lbs) | Cruise Altitude (Feet) | Flight Length (Minutes) |
|---|---|---|---|---|---|
| 1 | 7 | 6240 | 500 | 5000 | 25 |

The second profile is called the Severe or Grand Canyon Profile and consists of two individual flight profiles. Several Model 402s are used to conduct tours through the Grand Canyon. The flights are at low altitudes over mountainous terrain. The Severe Profile was developed to represent these Grand Canyon tour airplanes and was used for the analysis of both Model 402 through "B" and Model 402C aircraft. Tables 5 and 6 present the details of the Severe Flight Profiles.

TABLE 5. FLIGHT PROFILE DEFINITIONS SEVERE—MODEL 402 THROUGH "B"

| Flight Profile Number | Number of Persons Onboard | Ramp Weight (Lbs) | Ramp Fuel (Lbs) | Cruise Altitude (Feet) | Flight Length (Minutes) |
|---|---|---|---|---|---|
| 1 | 8 | 6331 | 661 | 7500 | 65 |
| 2 | 8 | 6064 | 394 | 8500 | 50 |

TABLE 6. FLIGHT PROFILE DEFINITIONS SEVERE—MODEL 402C

| Flight Profile Number | Number of Persons Onboard | Ramp Weight (Lbs) | Ramp Fuel (Lbs) | Cruise Altitude (Feet) | Flight Length (Minutes) |
|---|---|---|---|---|---|
| 1 | 9 | 6820 | 720 | 7500 | 65 |
| 2 | 9 | 6547 | 447 | 8500 | 50 |

The third profile set is called the Typical Usage Profile which consists of six individual flight profiles. These flight profiles were derived from the usage data collected from the surveys, minus the Short Flight and Grand Canyon operators. This data is represented by a three-parameter Weibull distribution as shown in figure 26. Six individual flight lengths were defined from the distribution curve to represent the overall flight length distribution as shown in figure 27. The Typical Usage Profile was used for both the Model 402 through "B" and the Model 402C aircraft. Tables 7 and 8 show the details of the Typical Usage Profiles.

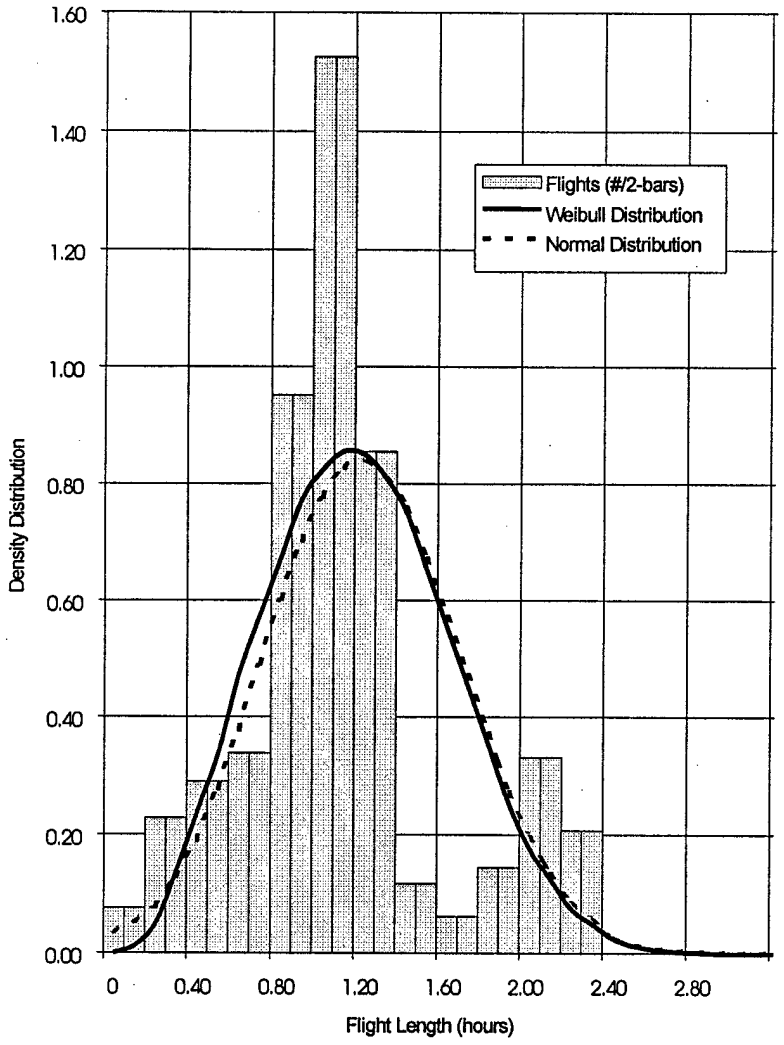


FIGURE 26. MODEL 402 FLIGHT LENGTH DISTRIBUTION—15 OF 17 OPERATORS

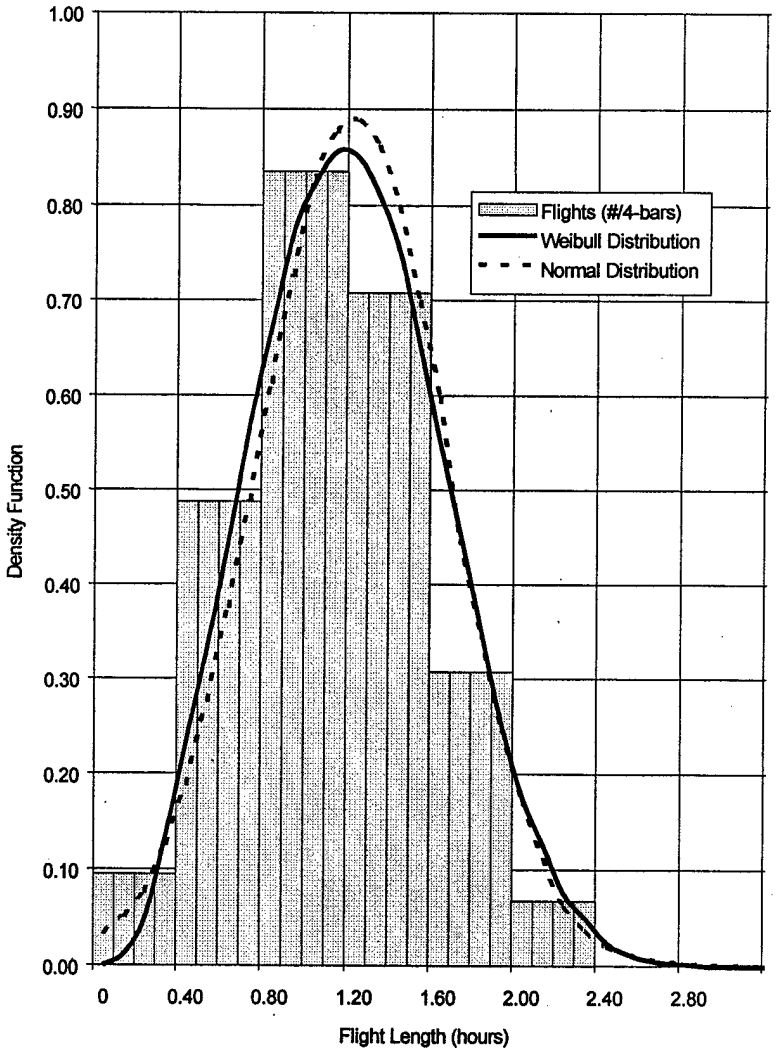


FIGURE 27. MODEL 402 FLIGHT LENGTH DISTRIBUTION

TABLE 7. FLIGHT PROFILE DEFINITIONS TYPICAL USAGE—MODEL 402 THROUGH "B"

| Flight Profile Number | Number of Persons Onboard | Ramp Weight (Lbs) | Ramp Fuel (Lbs) | Cruise Altitude (Feet) | Flight Length (Minutes) |
|---|---|---|---|---|---|
| 1 | 4 | 5928 | 978 | 5000 | 18 |
| 1 | 6 | 6062 | 932 | 7000 | 38 |
| 3 | 6 | 6052 | 742 | 7500 | 60 |
| 4 | 5 | 6137 | 1007 | 8000 | 83 |
| 5 | 6 | 6185 | 875 | 8300 | 106 |
| 6 | 8 | 6331 | 661 | 10000 | 128 |

TABLE 8. FLIGHT PROFILE DEFINITIONS TYPICAL USAGE—MODEL 402C

| Flight Profile Number | Number of Persons Onboard | Ramp Weight (Lbs) | Ramp Fuel (Lbs) | Cruise Altitude (Feet) | Flight Length (Minutes) |
|---|---|---|---|---|---|
| 1 | 6 | 6486 | 926 | 5000 | 18 |
| 2 | 7 | 6620 | 880 | 7000 | 38 |
| 3 | 8 | 6610 | 690 | 7500 | 60 |
| 4 | 9 | 6771 | 671 | 8000 | 83 |
| 5 | 8 | 6743 | 823 | 8300 | 106 |
| 6 | 9 | 6881 | 781 | 10000 | 128 |

The aircraft weight configurations for each of the flight profiles are presented in tables 9 and 10. For all Model 402 through "B" profiles, the basic empty weight is 4230 lb., which includes a 3950 lb. standard empty weight plus 280 lb. of optional equipment. The typical Model 402C basic empty weight is 4480 lb., which includes a 4200 lb. standard empty weight plus 280 lb. of optional equipment. Average passenger weight with baggage is assumed to be 180 lb. The center of gravity data was obtained from the respective pilot operating handbooks.

Each of the flight profiles defined was divided into several flight (mission) segments for which average altitudes, aircraft weights, and velocities were specified. These parameters were used to define the gust environment experiences for each flight profile. Cruise altitudes were based on information from the customer surveys. Flight velocities for climb, cruise, and descent were derived from the Model 402B and Model 402C pilot operating handbooks. Fuel consumption rates were also derived from the pilot operating handbooks.

TABLE 9. AIRCRAFT WEIGHT CONFIGURATION—MODEL 402 THROUGH "B"

| Configuration | Profile | Description |
|---|---|---|
| 1 | Severe Profile 1 | 1 pilot, 7 passengers, 600 lbs fuel in main tank, 61 lbs fuel in auxiliary tank. |
| 2 | Severe Profile 2 | 1 pilot, 7 passengers, 394 lbs fuel in main tank. |
| 3 | Typical Profile 1 | 1 pilot, 3 passengers, 600 lbs fuel in main tank, 378 lbs fuel in auxiliary tank. |
| 4 | Typical Profile 2 | 1 pilot, 5 passengers, 600 lbs fuel in main tank, 332 lbs fuel in auxiliary tank. |
| 5 | Typical Profile 3 | 1 pilot, 5 passengers, 600 lbs fuel in main tank, 142 lbs fuel in auxiliary tank. |
| 6 | Typical Profile 4 | 1 pilot, 4 passengers, 600 lbs fuel in main tank, 378 lbs fuel in auxiliary tank, 29 lbs fuel in wing locker. |
| 7 | Typical Profile 5 | 1 pilot, 5 passengers, 600 lbs fuel in main tank, 275 lbs fuel in auxiliary tank. |
| 8 | Typical Profile 6 | 1 pilot, 7 passengers, 600 lbs fuel in main tank, 61 lbs fuel in auxiliary tank. |

TABLE 10. AIRCRAFT WEIGHT CONFIGURATION—MODEL 402C

| Configuration | Profile | Description |
|---|---|---|
| 1 | Short Flight Profile | 1 pilot, 6 passengers, 500 lbs fuel in main tank. |
| 2 | Severe Profile 1 | 1 pilot, 8 passengers, 600 lbs fuel in main tank, 120 lbs fuel in auxiliary tank. |
| 3 | Severe Profile 2 | 1 pilot, 8 passengers, 447 lbs fuel in main tank, 61 lbs fuel in auxiliary tank. |
| 4 | Typical Profile 1 | 1 pilot, 5 passengers, 600 lbs fuel in main tank, 326 lbs fuel in auxiliary tank. |
| 5 | Typical Profile 2 | 1 pilot, 6 passengers, 600 lbs fuel in main tank, 280 lbs fuel in auxiliary tank. |
| 6 | Typical Profile 3 | 1 pilot, 7 passengers, 600 lbs fuel in main tank, 90 lbs fuel in auxiliary tank. |
| 7 | Typical Profile 4 | 1 pilot, 8 passengers, 600 lbs fuel in main tank, 71 lbs fuel in auxiliary tank. |
| 8 | Typical Profile 5 | 1 pilot, 7 passengers, 600 lbs fuel in main tank, 223 lbs fuel in auxiliary tank. |
| 9 | Typical Profile 6 | 1 pilot, 8 passengers, 600 lbs fuel in main tank, 181 lbs fuel in auxiliary tank. |

Each of the profiles was broken into the separate flight segments as follows:

- Taxi to runway—Occurs at a weight midway between ramp and takeoff.
- Climb—The total number of climb segments depends on the final cruise altitude. Each segment represents no more than a 5,000 ft. change and the other parameters used represent an average during that segment.
- Cruise—The total number of cruise segments depends on the total time spent in cruise. Each segment will represent no more than 25 minutes and the other parameters used represent an average during that segment.
- Descent—The segments are defined in the same manner as the climb phase.
- Approach—This is the last descent segment prior to touchdown. The velocity is limited to 102 knots calibrated airspeed (KCAS).
- Maneuvers—Parameters are identical to the approach segment. In general, most maneuvering done with an aircraft of this class can be expected to be done just after takeoff and prior to landing. Of these, the maneuvers prior to landing could be expected to be the more frequent and for that reason all maneuvers will be assumed to take place during the approach segment.
- Approach-to-Landing Flap Deflection—Parameters are identical to the approach segment with the exception of deflected flaps at 15° and 45°.
- Landing Impact—Uses parameters at moment of touchdown. This segment is used to calculate the gear loads at touchdown.
- Taxi to Ramp—Handled the same as the initial taxi segment and occurs at a weight midway between touchdown and engine shut down.

2.3.3 Load Spectra Development.

The load spectra for the Model 402 damage tolerance analyses are presented in two categories: those spectra affecting the major airframe components and those specifically affecting the landing gear. The airframe load spectra is presented in section 2.3.3.1 and the landing gear load spectra is presented in section 2.3.3.2.

2.3.3.1 Airframe Load Spectra.

The aircraft flight profile load parameters were calculated using the defined flight profiles and the aircraft weight configuration data. Center of gravity (c.g.) was calculated for all flight load segments of the profiles defined for specific passenger and fuel loading and passenger and fuel weight distribution. The flight profile load parameters include fuel weights in the separate fuel tanks, gross weights, flight speed, flight mach number, flight altitudes, c.g. location, thrust, and length of each flight segment. These load parameters were used to calculate load spectra.

Table 11 summarizes the load spectra considered in the damage tolerance evaluation of all major airframe components in conjunction with the flight profiles and aircraft configurations defined in section 2.3.2. The load spectra are discussed in more detail in the following paragraphs.

TABLE 11. AIRFRAME LOAD SPECTRA

| Major Airframe Component | Load Spectra to be Considered |
|---|---|
| Wing and Carry-Thru | Maneuver, vertical gust, landing impact, taxi, ground-air-ground |
| Fuselage | Maneuver, vertical and lateral gust, landing impact, taxi, ground-air-ground |
| Empennage | Maneuver, vertical and lateral gust, balancing tail load cycles, landing impact, taxi, ground-air-ground |
| Engine Support | Maneuver, vertical gust, landing impact, taxi, engine thrust, ground-air-ground |

The Model 402 analytical maneuver spectrum was based on an accumulation of data from references 5, 6, and 7. The maneuver spectrum was defined by constructing a conservative curve through the data points as shown in figure 28. Load cycles and occurrences were defined from these curves by combining positive and negative incremental load factors at the same exceedance level. In the absence of a rational approach to vertical tail maneuver spectra, vertical tail maneuver loading for fatigue evaluation was accounted for in the gust spectrum.

The vertical gust load spectrum for the Model 402 was defined in terms of aircraft center of gravity accelerations (i.e., vertical load factor, $N_z$) for each of the flight profiles defined. A comparison was made of vertical load factor exceedance data compiled from references 5, 6, and 8 as presented in figure 29. Based on this comparison of exceedance data, the Model 402 was evaluated using the ESDU data of reference 8. This data is a compilation of normalized gust exceedances obtained from several different aircraft using the velocity load factor altitude (VGH) method.

The lateral gust load spectrum for the Model 402 fatigue evaluation was defined in terms of gust velocity exceedances. This spectrum was developed from reference 8 data assuming that the overall gust environment is isotropic. In addition, a lateral gust in one direction was assumed to be followed by one of equal magnitude in the opposite direction. In the absence of a rational vertical tail maneuver spectrum and a dynamic analysis of the empennage response to gust spectrum, an occurrence factor of two was applied to lateral gust occurrences to account for maneuver loadings and the dynamic response of the empennage to lateral gusts as recommended in reference 9.

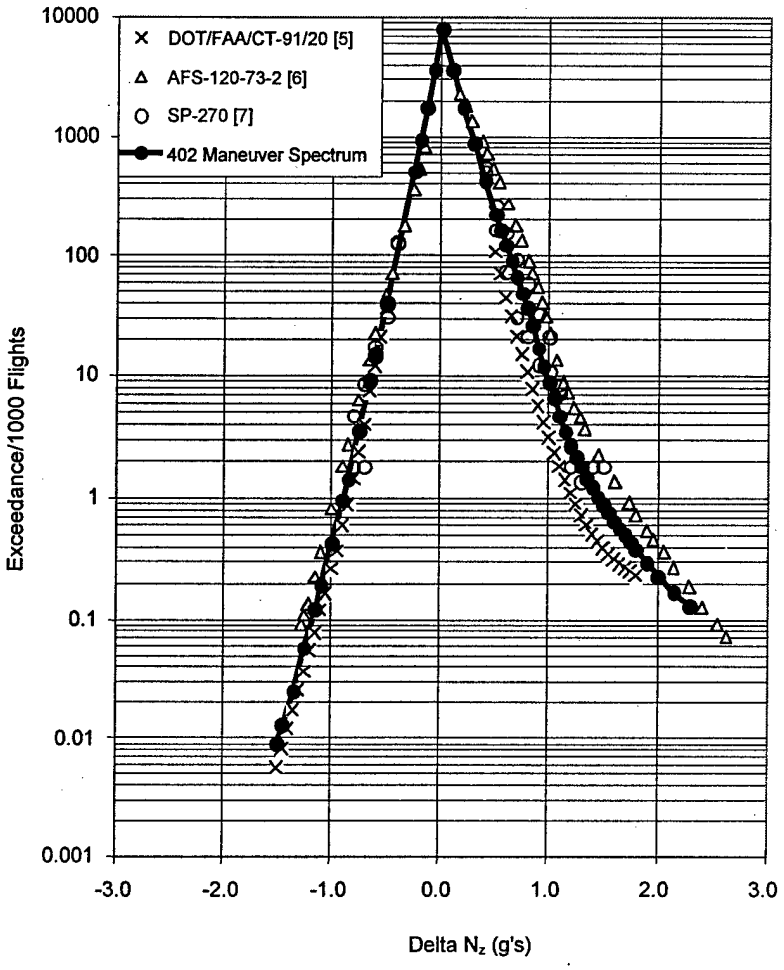


FIGURE 28. MODEL 402 MANEUVER SPECTRUM

The Model 402 taxi spectrum (vertical load) was derived in terms of vertical load factor ($N_z$) occurrences at the aircraft center of gravity per 1000 flights. The spectrum was based on data from reference 6, as shown in figure 30.

During the strain survey (section 2.3.4), a variety of landings were recorded representing a max-min range of recorded $N_z$ values from 1.3-0.7 to 2.2-0.2. Landing strains were extracted from the flight strain survey in a time history format for each strain gauge. The recorded stresses were used directly in the stress spectrum. The number of occurrences of each recorded landing in the spectra was selected to parallel the usage spectrum defined in reference 6, as shown in figure 31.

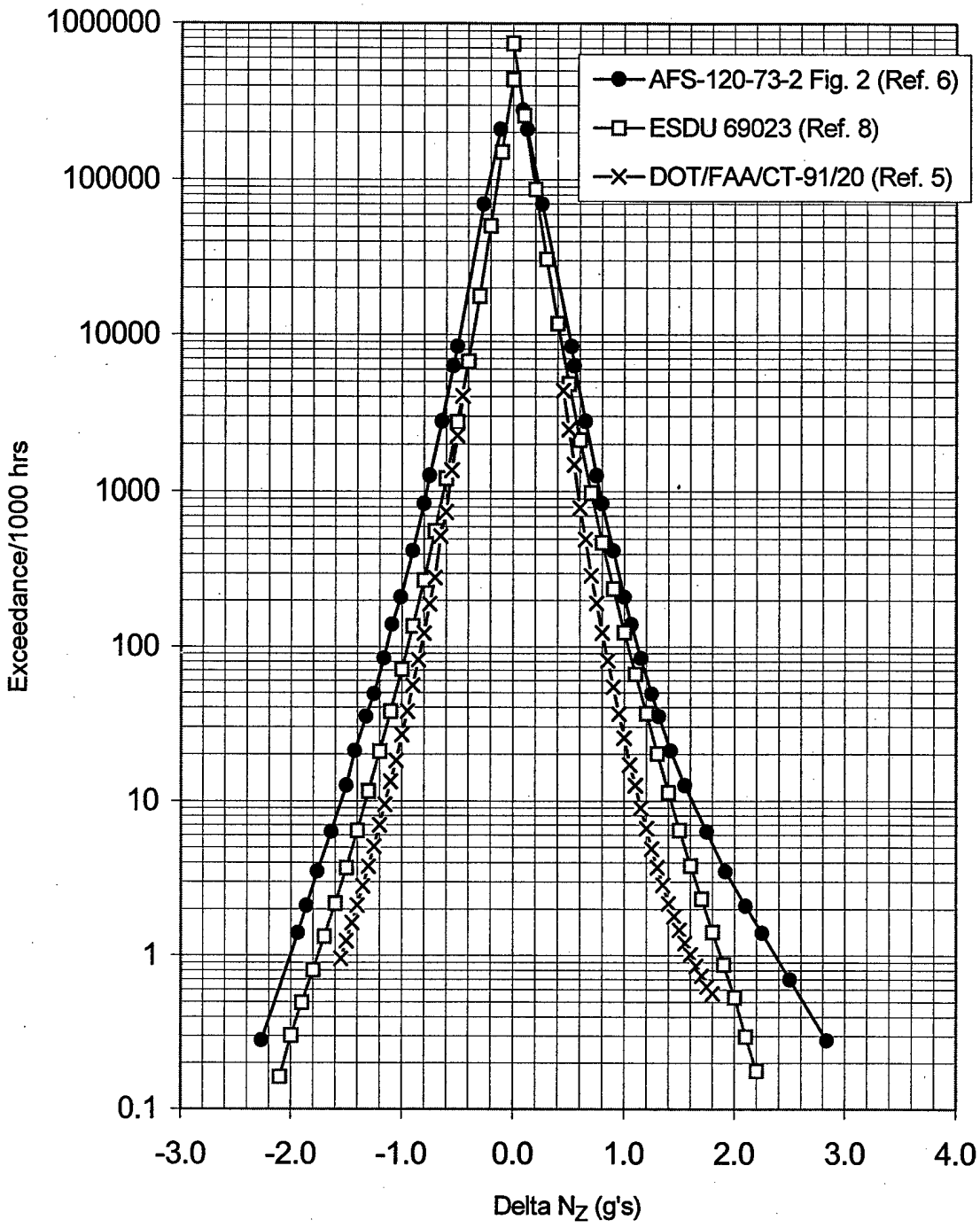


FIGURE 29. MODEL 402 VERTICAL GUST LOAD EXCEEDANCE COMPARISON

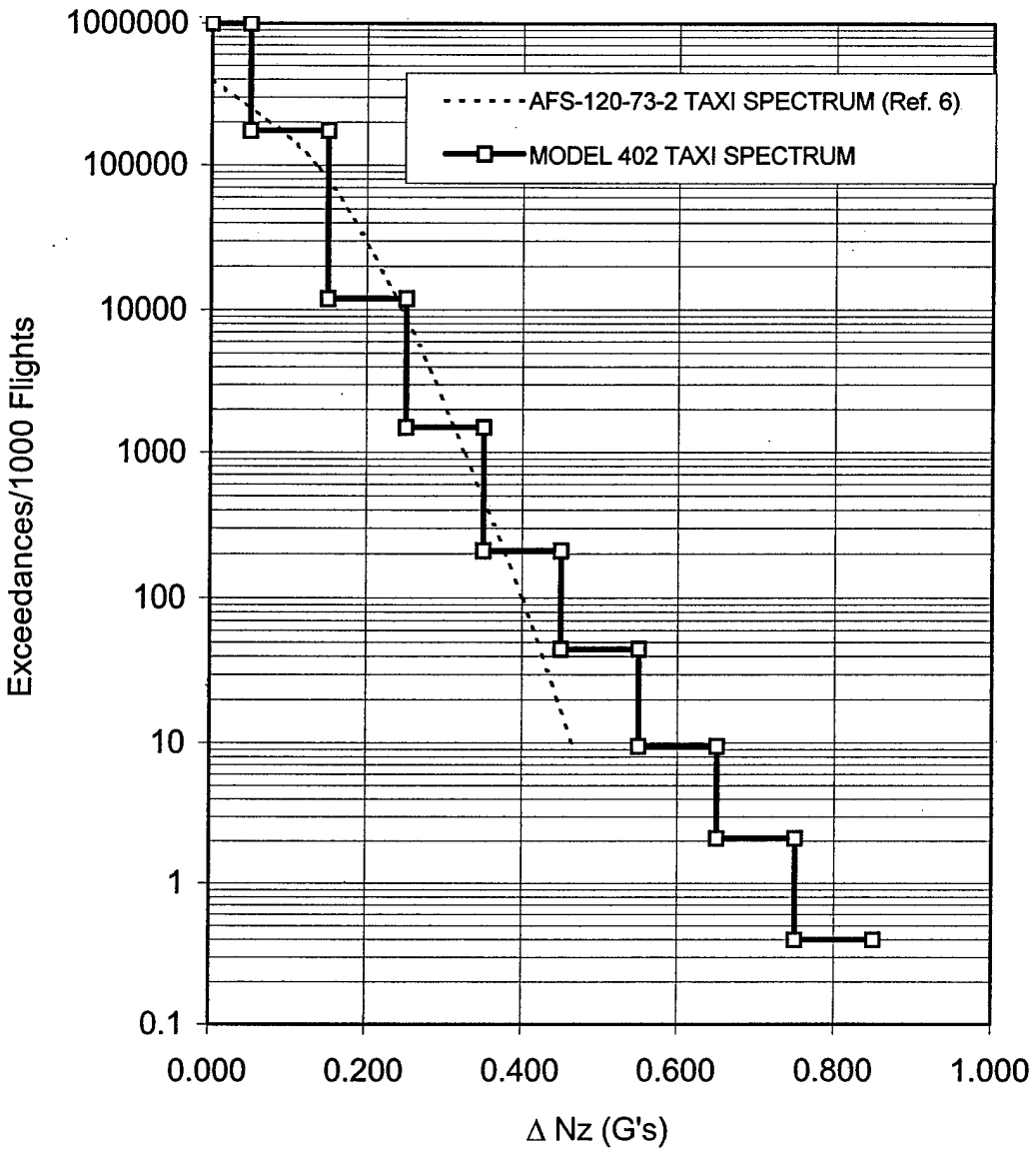


FIGURE 30. MODEL 402 TAXI SPECTRUM

The ground-air-ground spectrum, employed in the wing and fuselage cabin analysis, is defined as the stress cycle per flight encompassing the maximum flight stress excursion and the minimum ground stress excursion. In the evaluation of fatigue loadings on the empennage, an additional loading cycle similar in definition to the ground-air-ground cycle was accounted for. The additional cycle, the overall residue cycle (ORC), is defined as the cycle encompassing the maximum positive stress and the maximum negative stress per flight. A procedure similar to the method used to compute ground-air-ground cycles was employed to determine ORC cycles for fatigue analysis.

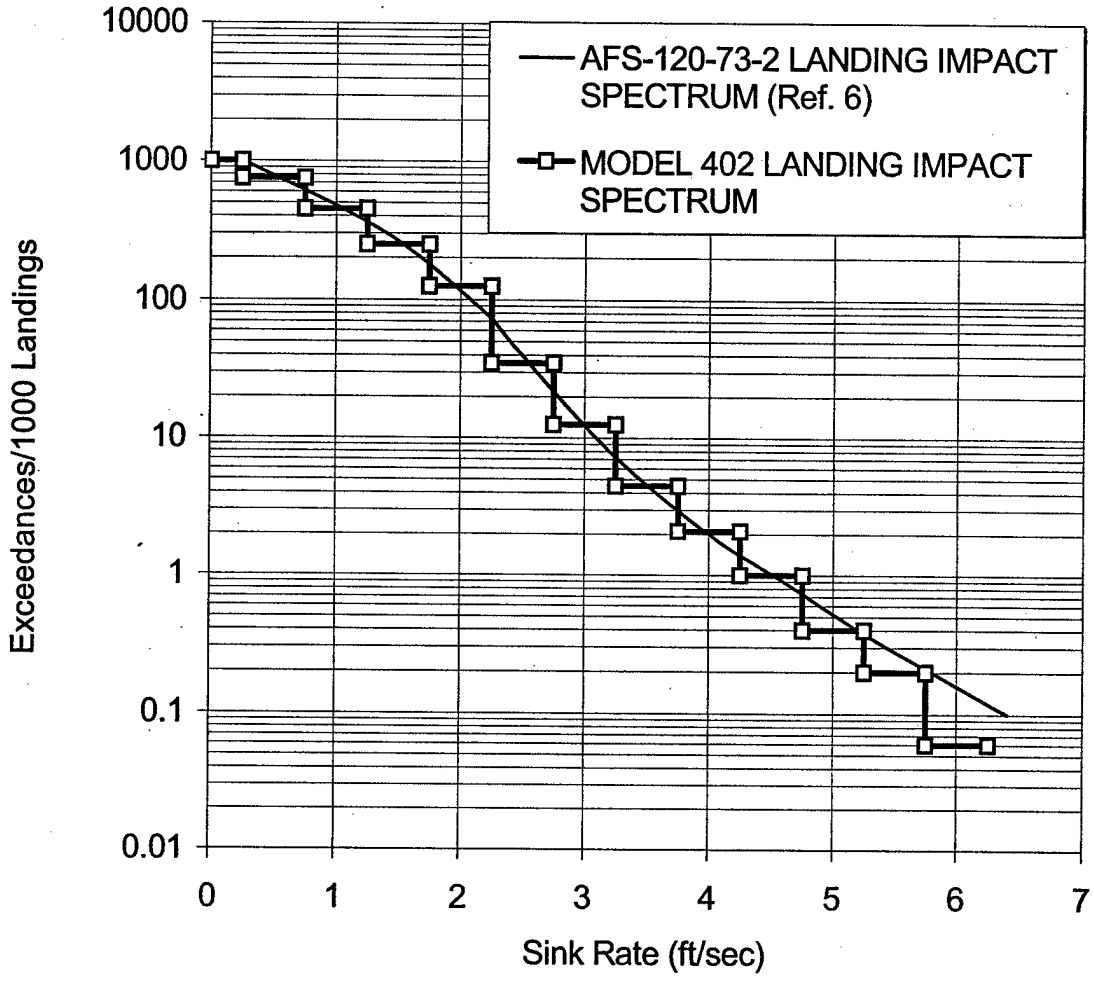


FIGURE 31. MODEL 402 LANDING IMPACT SPECTRUM

For each of the profiles defined the horizontal stabilizer was investigated for stress cycles resulting from changes in one g balancing loads due to velocity change and flap position changes.

The effects of engine thrust are considered in the fatigue evaluation of the airframe. Specific thrust values for the individual flight segments of section 2.3.2 were calculated using the engine rpm and manifold pressure.

The Model 402 is unpressurized; therefore, the effects of cabin pressure were not considered.

2.3.3.2 Landing Gear Load Spectra.

The landing gear spectra along with finite element stress equations and methods established for calculation of gear loads in reference 10 were used to develop the Model 402 main landing gear fatigue analysis. The spectra for the Model 402 landing gear analysis include the following:

- Landing Impact
- Taxi
- Turning
- Braking
- Pivoting

The taxi and landing impact spectra were based on data from reference 6, as shown in figures 30 and 31. The Model 402 turning load spectrum was defined in terms of lateral acceleration (LACG) occurrences at the aircraft center of gravity. The turning load spectrum was derived from data collected by Cessna and presented in reference 10. The Model 402 braking load spectrum was also derived from reference 10 in terms of brake load/1000 lb. gross weight occurrences. The pivoting spectrum for the Model 402 included two rolling pivots per flight, one pivot prior to takeoff and one prior to engine shutdown after taxi-in.

2.3.4 Flight Strain Survey.

A flight strain survey program was undertaken to determine stress equations as a function of flight parameters for use in damage tolerance stress spectra development. A Model 402C aircraft was acquired, instrumented, and flown under a variety of representative conditions in order to record enough data to perform statistical regressions. The aircraft was instrumented with 51 strain gauges, vertical and lateral accelerometers near the aircraft c.g., and lateral accelerometers near the vertical fin center of pressure (c.p.). Airspeed was already available in the aircraft instrumentation package. The aircraft gross weight, fuel weight, altitude, indicated airspeed, left/right engine speed (rpm), left/right engine manifold pressure, and flap position were all manually recorded by an observer during the flights.

In order to record sufficient data variation to obtain confidence in the regressions, the aircraft was flown with two different zero fuel weight configurations and various wing fuel loading. Airspeed and altitude were varied to the full range of expected values. Flight conditions for gust, coordinated maneuvers, taxis, and landings were performed. Gusts were flown at different airspeeds ranging from approximately 130 KCAS indicated to 190 KCAS for each of the loading configurations. The maneuvers were symmetric (or nearly symmetric) steady-state load conditions including left/right wind-up turns, push-overs, and roller coasters. Taxis were performed over relatively rough runways for each of the weight configurations. Landings were performed for each weight range and included normal and hard landings.

The data were reviewed to identify good data streams as well as data which looked erroneous or included non-steady-state maneuvers. Valid data streams were selected and extracted from the tapes and stored for regression. The flight data were regressed to specified stress equations using a linear least squares regression technique. Statistical parameters computed include correlation coefficient, standard error on coefficient, t-statistic on coefficient, residual distribution, cumulative frequency of residuals, and computed vs. actual values. Stress equations were regressed for vertical and lateral gust, maneuvers using 0° or 15° flaps, maneuvers using 45° flaps, taxi alternating stress and taxi mean stress. Landing strains were extracted in a time

history format for direct use in the spectrum. Obvious data spikes or errors were extracted from the samples resulting in significant correlation improvements.

Gust stress equations were regressed in an alternating stress format. Root mean square (RMS) stresses and corresponding RMS load factors were computed over several seconds to determine the deviation stress resultant. As the cycles of stress and load factors are not necessarily equivalent, the ratio of stress cycles to load factor were also computed for use in the spectra development. The load factor used for vertical gust (horizontal tail and engine beams) is $N_z$ while the load factor used for lateral gusts (vertical tail and tailcone) is $N_y$ at the fin.

Symmetric maneuver stress equations were developed in an absolute stress format. Normally the stress equations are developed for any flap setting (e.g., 0°, 15°, 45°). For this aircraft, the landing gear is extended for all flap extensions above 15°. The change in aircraft attitude necessitates a separate equation for 45° flap conditions.

Taxi mean and alternating stress equations used the same strain survey sample database. The taxi mean stress equations were absolute stress format while the taxi alternating stress equations were in an alternating (or deviation) format similar to gust.

2.3.5 Stress Spectra Development.

2.3.5.1 Stress Equations.

Stress equations were developed for the taxi, maneuver, and gust flight segments defined in the Model 402 Load Spectra using the stresses obtained from the flight strain survey of the Model 402. Two adjustment factors were applied to the stress equations to obtain the stresses at the analysis locations. The adjustment factors developed are defined as the net area factor (NAF) and the transfer factor (TF).

A net area factor was applied to the basic stress equation to account for the reduction in cross-sectional area due to the absence of material at fastener locations. The NAF was calculated by dividing the gross cross-sectional area by the net-sectional area. Net area stresses were used for classical fatigue damage analyses only. The crack growth analyses used gross area stresses.

A transfer factor was defined to transfer the stress from the strain gauge location to the analysis location. TF was found by dividing the stress at the analysis location by the stress at the strain gauge location as determined from the NASTRAN finite element model.

Segment-by-segment stress equation coefficients for all profiles and analysis locations were determined. The following symbols and definitions were used in the stress equation development:

$\sigma$ = Stress, psi

$\frac{\Delta \sigma}{\Delta N_z}$ = Incremental Gust Stress, psi/g

$N_z$ = Normal Acceleration at Aircraft Center of Gravity, g

$C_1$ = Coefficient of $N_z$ in Stress Equation, psi/g

$C_3$ = Constant Term in Stress Equation, psi

Subscripts:

t = Taxi
m = Maneuver
g = Gust
alt = Alternating component
mean = Mean component
ss = Steady state component

2.3.5.1.1 Taxi Stress Equation.

The taxi stress $T_t$ was defined as a mean stress, $\sigma_{t_{mean}}$, plus an alternating component, $\sigma_{t_{alt}}$. These terms were expressed as a function of several variables such as wing fuel weight, gross weight, and c.g. location. The taxi stress can be represented as

$$\sigma_t = \sigma_{t_{alt}} + \sigma_{t_{mean}}$$

$$= \frac{\sigma_t}{\Delta N_Z} \cdot \Delta N_Z + \sigma_{t_{mean}}$$

$$= \frac{\sigma_t}{\Delta N_Z} \cdot (N_Z - 1) + \sigma_{t_{mean}}$$

$$= \frac{\sigma_t}{\Delta N_Z} \cdot N_Z - \frac{\sigma_t}{\Delta N_Z} + \sigma_{t_{mean}}$$

The stress equation was rewritten as

$$\sigma_t = C_{1_t} \cdot N_Z + C_{3_t}$$

where

$$C_{1_t} = \frac{\sigma_t}{\Delta N_Z}$$

$$C_{3_t} = - \frac{\sigma_t}{\Delta N_z} + \sigma_{t_{mean}}$$

2.3.5.1.2 Maneuver Stress Equation.

The maneuver stress equation was developed as a steady-state condition based on several variables such as wing fuel weight, gross weight, and equivalent airspeed. The maneuver stress $T_m$ can be represented as

$$\sigma_m = \frac{\sigma_m}{N_z} \cdot N_z + \sigma_{mss}$$

where

$\frac{\sigma_m}{N_z}$ = stress per g in normal direction, psi/g

$\sigma_{mss}$= steady-state stress, psi

The equation can be rewritten as

$$\sigma_m = C_{1_m} \cdot N_z + C_{3_m}$$

where

$$C_{1_m} = \frac{\sigma_m}{N_z}$$

$$C_{3_m} = \sigma_{mss}$$

2.3.5.1.3 Gust Stress Equation.

The gust stress equation was developed as a change in gust stress per change in normal acceleration, $\frac{\Delta \sigma_g}{\Delta N_z}$, plus a 1 g steady-state stress, $\sigma_{ss}$. The maneuver stress at 1 g was used to develop $\sigma_{ss}$. The gust stress $t_g$ was represented as

$$\sigma_g = \frac{\Delta \sigma_g}{\Delta N_z} \cdot \Delta N_z + \sigma_m@1g,$$

Since

$$\Delta N_Z = N_Z - 1 \text{ and } \sigma_m@1g = C_{1_m} + C_{3_m},$$

$$\sigma_g = \frac{\Delta \sigma_g}{\Delta N_Z} \cdot N_Z - \frac{\Delta \sigma_g}{\Delta N_Z} + C_{1_m} + C_{3_m}$$

This equation was rewritten as

$$\sigma_g = C_{1_g} \cdot N_Z + C_{3_g}$$

where

$$C_{1_g} = \frac{\Delta \sigma_g}{\Delta N_Z}$$

$$C_{3_g} = C_{1_m} + C_{3_m} - \frac{\Delta \sigma_g}{\Delta N_Z}$$

2.3.5.2 Stress Spectra.

The Model 402 flight-by-flight stress spectra used in the crack growth analyses were derived from the load spectra and the gross area stress equations. In generating the stress spectra, the following procedure was used for each profile:

a. Stresses were calculated on a gross area stress basis. The associated number of cycles in each segment was determined on a flight basis with segments arranged in sequence (i.e., taxi-out, climb gust, cruise gust, descent gust, maneuver, and taxi-in).

b. No truncation was performed for flight segments. A once-per-flight taxi loading, which is necessary for the ground-air-ground transition, was retained.

c. The number of occurrences of each stress cycle in the spectrum was rounded to a whole number. Fractional occurrences less than 0.5 were summed and rounded to the nearest whole number.

d. Each flight profile was expanded into four flights, one including stresses which occur once per flight, one including stresses which occur once per ten flights, one including stresses which occur once per hundred flights and one including stresses which occur once per thousand flights. The 1/10, 1/100, and 1/1000 flights were created by successively multiplying the occurrences by ten and adding the digit to the left of the

decimal point to the original number of occurrences. For example, if the occurrences for the stress level were 15.2964 then the 1/1 flight would have 15 occurrences; the 1/10 flight would have 15+2=17 occurrences; the 1/100 flight would have 17+9=26 occurrences; and the 1/1000 flight would have 26+6=32 occurrences. When creating the 1/1000 flight, the number to the right of the decimal point (in this example d) is considered. If it is less than 0.5, it is truncated. If it is 0.5 or greater, it is used to round up to the whole number.

e. The stresses within each flight were cycle counted. The particular cycle counting method used for the Model 402 is referred to as the NLR method. It closely resembles the range-pair and rainflow counting methods. The NLR method given in reference 11 was modified so that the maximum stresses occur in the same order as in the actual spectrum.

## 3. PHASE 2 TASKS.

### 3.1 COLLECT MATERIAL PROPERTY DATA.

The first step in conducting the damage tolerance analyses of the Model 402C and Model 402 through "B" airframes was to locate the required material properties for each component of the airframe. An extensive search was done to locate the required material properties which included Cessna generated material data and published data from industry sources.

#### 3.1.1 Material Properties.

For crack growth and/or residual strength analyses, several material properties are required. These material properties include the following:

- Yield Strength
- Ultimate Tensile Strength
- Modulus of Elasticity
- Fracture Toughness
- Fracture Threshold $\Delta K_{th}$
- Fatigue Endurance Limit
- Stress Ratio Cutoff Behavior
- Crack Growth Rate - da/dN vs. $\Delta K$
- Willenborg-Chang Shut-off Ratio

The material parameters required for crack growth for the materials used in the Model 402C and/or Model 402 through "B" airframes are documented in appendix A of reference 3. An example of the material properties documented in this reference is shown in table 12.

TABLE 12. MATERIAL PROPERTIES: 2014-T6 EXTRUSION [3]

Static Strength, ksi

| | | |
|---|---|---|
| $F_{tu}$ | 60 | (1) |
| $F_{ty}$ | 53 | (1) |

Modulus of Elasticity, $10^3$ ksi

| | | |
|---|---|---|
| E | 10.8 | (2) |

Fracture Toughness, ksi$\sqrt{in}$

| | | |
|---|---|---|
| $K_{Ic}$ | 27.9 | (3) |
| $K_c$ | 65.0 | (4) |

Crack Growth Threshold Data

| | | |
|---|---|---|
| $\Delta K_{th0}$ | 2.38 | (5) |
| A | 0.833 | (5) |
| $\Delta\sigma_e$ | 18 | (6) |

NASGRO 2.0 da/dN Equation Constants (7)

| | C | n | p | q |
|---|---|---|---|---|
| Single Slope | 0.350E-7 | 2.800 | 0.5 | 1.0 |

da/dN is taken directly from the FLAGRO Database with R values of -1.0, -.5, 0, .3, .4, .5, .6, .7, .8, .9

Willenborg-Chang Load Interaction Shut-off Ratio

| | | |
|---|---|---|
| $R_{SO}$ | 2.30 | (8) |

1. Reference 16, pg. 3-33 (L, A basis, AMS 4153 & QQ-A-200/2).
2. Reference 16, pg. 3-33 (tension).
3. Reference 17, pg. 7.0-7, assumed same as 2014-T6 forging, L-T mean value.
4. Reference 17, pg. 7.0-9 & 7.0-10, 2014-T6 , L-T average value.
5. Reference 12, pg. 5-3
6. Reference 18 , pg. 299
7. Reference 13, pg. G1-9, assumed same as 2014-T6 plate, L-T value.
8. Reference 19, pg. 722.

3.1.2 Material Testing.

Material tests were defined for those materials for which reliable industry data or previously existing Cessna data could not be found. Three types of tests were conducted and are addressed in the following sections.

3.1.2.1 Crack Growth Rate Data (da/dN) Tests.

Da/dN data, required to conduct the crack growth analyses, were located from Cessna or industry sources for all of the required materials except for 301 (1/4 hard) steel. Da/dN coupon tests were conducted to obtain the necessary data for this material. In addition, da/dN coupon tests were conducted for 7075-T6 material, so that da/dN could be eliminated as a variable in spectrum testing.

Three lots of 0.032" thick 301 (1/4 hard) steel were obtained. From each lot of material, six coupons were made and tested. Test coupons for da/dN testing were fabricated in compliance with the standard of ASTM E647-88a, "Standard Test Method for Measurement of Fatigue Crack Growth Rates" [20]. Grain directions were marked on the sheets to assure proper testing in the T-L direction. The coupons were tested at different R-ratios ranging from .05 to .70. The tests were conducted at room temperature and high humidity air under constant load. An outside vendor was contracted to complete the testing.

One lot of 0.25" thick 7075-T6 Extrusion was obtained. Six coupons were made in compliance with the standard of ASTM E647-88a [20] for da/dN testing. Two coupons each were tested at R-ratios of .10, .40, and .70. The tests were conducted at room temperature and high humidity air under constant load. The tests were conducted at Cessna.

Da/dN vs. $\Delta$ K plots were constructed using the seven point polynomial technique per ASTM E647 for each coupon. A tri-slope Walker equation was developed which best fit the data. The test results are presented in appendix A of reference 3. Laboratory evaluations were also performed to establish the standard acceptability of the 301 (1/4 hard) steel and the 7075-T6 aluminum materials.

3.1.2.2 Fracture Toughness ($K_c$) Tests.

Fracture toughness ($K_c$ or $K_{1c}$) data, required to conduct the crack growth analyses, were located from Cessna or industry sources for all of the required materials except for 301 (1/4 hard) steel. Fracture toughness ($K_c$) tests were conducted to obtain the necessary data.

Three 16" wide panels, one each from three different lots of 0.032" thick 301 (1/4 hard) material were tested. Grain directions were marked on the sheets to assure proper testing in the T-L direction. The tests were run in accordance with the requirements of ASTM E561, "Standard Practice for R-Curve Determination" [21], using the center-cracked tension panel M(T). Since all testing for $K_c$ was done using 16-inch-wide center-cracked coupons, the derived $K_c$'s are less than the actual material $K_c$ value. Even so, the values are considered appropriate as they compare better to the panel widths used in the analyses. The test results are presented in appendix A of reference 3.

3.1.2.3 Spectrum Loaded Coupon Tests.

Spectrum loaded coupon tests were conducted to establish crack growth retardation effects for the wing and empennage locations considered to be the most critical for crack growth life. The

Willenborg-Chang retardation model was chosen for crack growth analyses of the Model 402 airframe. The Willenborg-Chang model reduces basic material crack growth rates using an equation involving plastic zone sizes at the crack tip. This model scales overload effects with a shut-off ratio ($R_{so}$) and has the ability to reduce the effective overload interaction zone for compressive stresses. The value of $R_{so}$ varies with material and with the stress ratio. Since a set of overload shut-off ratios for random spectrum loadings is impractical in life prediction, a single value of $R_{so}$ is used. These tests were conducted to verify that the published values of $R_{so}$ for the Willenborg-Chang crack growth equation are conservative. A summary of the locations which were tested, and the corresponding value of $R_{so}$ is presented in table 13.

TABLE 13. SUMMARY OF TEST LOCATIONS

| Aircraft Model | Aircraft Component | Location and Description | $R_{so}$ |
|---|---|---|---|
| 402 Through "B" | Wing | BW-5, Wing Lower Front Spar Cap, W.S. 75.66 | 2.65 |
| | | BW-6, Wing Lower Front Spar Cap at Inboard Engine Beam Attach, W.S. 83.74 | 2.65 |
| 402C | Wing | CW-2, Wing Lower Front Spar Cap at Root Fitting Attach, W.S. 66.70 | 2.65 |
| | | CW-3, Wing Lower Front Spar Cap at Canted Rib Attachment, W.S. 80.84 | 2.65 |
| | | CW-5, Wing Lower Front Spar at Outboard Engine Beam Attach, W.S. 107.02 | 2.65 |
| | Horizontal Stabilizer | CH-1, Horizontal Stabilizer Forward Spar Upper Cap, B.L. 0.0 | 2.30 |

Axially loaded coupons (4″ wide x 16″ long) with a center hole flawed on both sides were used to conduct the tests. The coupons were fabricated in compliance with the standards of ASTM E647-88a [20]. The materials used to fabricate the coupons are the same as used in the Model 402C and Model 402 through "B" aircraft and the coupon thickness is the same as for the corresponding airframe locations. Moreover, the materials used for these spectrum coupon tests are from the same stock as used for da/dN vs. $\Delta K$ crack growth curve determination, which eliminates variability in da/dN data as a factor in retardation.

The test coupons were precracked to a length of 0.14 inch by applying constant amplitude stress cycles. The objective of the precrack is to produce a sharp fatigue crack to facilitate crack growth during spectrum loading. After precracking, flight-by-flight loading was applied to each test coupon to duplicate the analytical gross area stress spectra at the structural location being tested. Crack growth was monitored as a function of the number of flight hours completed.

The actual crack growth measured experimentally by applying the flight-by-flight spectrum to the test coupon was plotted to obtain the test crack growth curve. The analytical crack growth, with and without retardation, were plotted with the experimental curve. The results of these

comparisons are presented in appendix A of reference 3. The test results verified that the published values of $R_{so}$ for the Willenborg-Chang crack growth equation are conservative.

## 3.2 ESTABLISHMENT OF INITIAL FLAW SIZES FOR EACH CRITICAL LOCATION.

The initial (pre-existing) and maximum (uninspectable) flaw shapes, sizes, and local orientation assumed for the damage tolerance analysis are presented in this section. The flaws are intended to provide the basis for analytical crack growth predictions to determine the initial and recurring inspection requirements for the aircraft.

The initial flaws defined in this section are identified as either primary or secondary flaws. Primary flaws are intended to provide the primary crack initiation site in a part and are representative of gross manufacturing defects. Secondary flaws are intended to provide the crack initiation site(s) for continuing growth after primary growth is arrested by growth to the edge of the part or into an adjacent hole. Secondary flaws are representative of typical manufacturing quality.

### 3.2.1 Primary Flaws.

Initial (primary) flaws are assumed to exist in the aircraft from the time of manufacture. These flaws, along with their subsequent growth under flight conditions, will establish the initial inspection times for the aircraft based on crack growth. The initial flaws are assumed to exist at holes, edges of cutouts, or edges of parts and exist at the most unfavorable location and orientation with respect to the applied stresses and material properties. The initial flaw size is the same regardless of whether the crack originates at a hole or if the crack originates at the edge of a part. These flaws will be quarter-circular corner cracks, except when the part thickness is less than or equal to the initial flaw size, in which case the flaw will be a through-the-thickness crack. The initial cracks will be assumed to start from the side of the hole nearest the edge of the part (when an edge of a part is present). The initial flaw sizes, based on AFGS-87221A [15], are presented in table 14 and shown in figure 32.

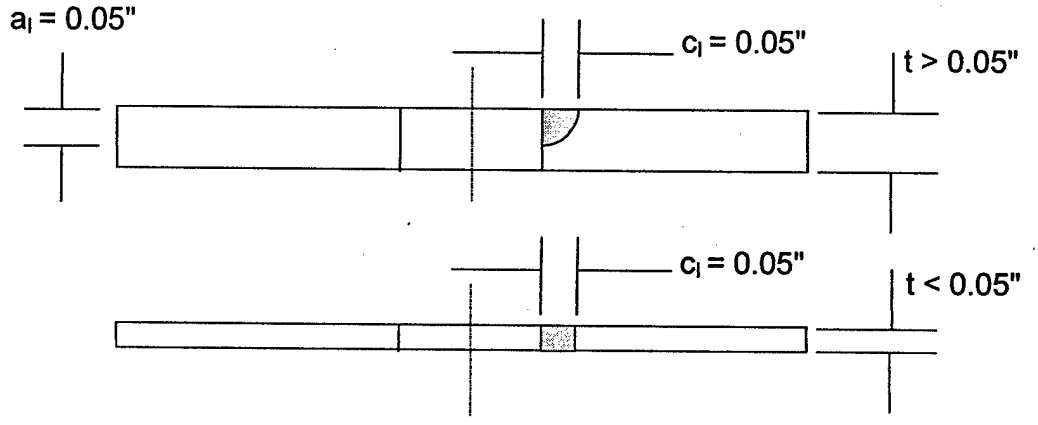


FIGURE 32. PRIMARY FLAW SIZE ASSUMPTIONS FOR HOLE/EDGE FLAW LOCATION

For locations away from holes, cutouts, or edges of parts, initial flaws will be semicircular surface flaws except where the part thickness is less than or equal to the initial flaw size, in which case they will be considered through the thickness. The initial flaw sizes for surface flaws are shown in table 14 and figure 33.

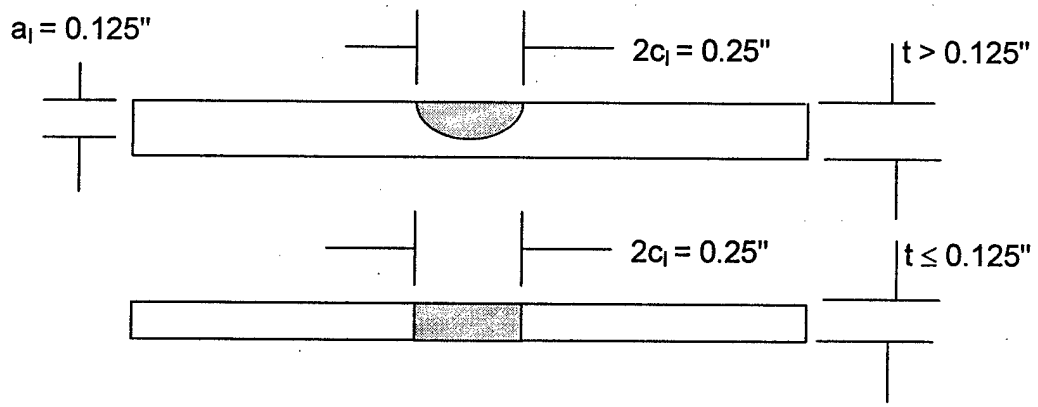


FIGURE 33. PRIMARY FLAW SIZE ASSUMPTIONS FOR SURFACE FLAW LOCATION

TABLE 14. PRIMARY FLAW SIZE ASSUMPTIONS

| Flaw Location | Flaw Shape | Thickness t - in. | $c_i$ - in. | $a_i$ - in. |
|---|---|---|---|---|
| Hole/Edge | Part Through | > 0.05 | 0.05 | 0.05 |
| Hole/Edge | Through | ≤ 0.05 | 0.05 | t |
| Surface | Part Through | > 0.125 | 0.125 | 0.125 |
| Surface | Through | ≤ 0.125 | 0.125 | t |

Only a single primary flaw will be assumed to exist at each location analyzed. However, in those cases where manufacturing operations exist such that a common flaw could exist in more than one element (common drilled holes), then a primary flaw will be assumed to exist in each element. If however, a common hole is drilled through multiple lug fittings and then each hole is individually dressed, as with a bushing, then only one element will be assumed to contain the initial flaw.

3.2.2 Secondary Flaws.

Secondary flaws will be assumed to grow independently of the primary flaw up to the point that the primary flaw induces a failure. During the time that it takes a primary flaw to grow from a fastener hole to the edge of the part (ligament failure), a secondary flaw will be assumed to be growing opposite the primary flaw. At failure of the ligament, the continuing damage will include the growth of the secondary crack. For dual load path members, after the failure of the member which contains the assumed primary flaw, the second member must have enough residual strength to support the load in the presence of a secondary flaw that has grown during

the time it took the other member to fail. The secondary flaw sizes for all structure are as shown in figure 34.

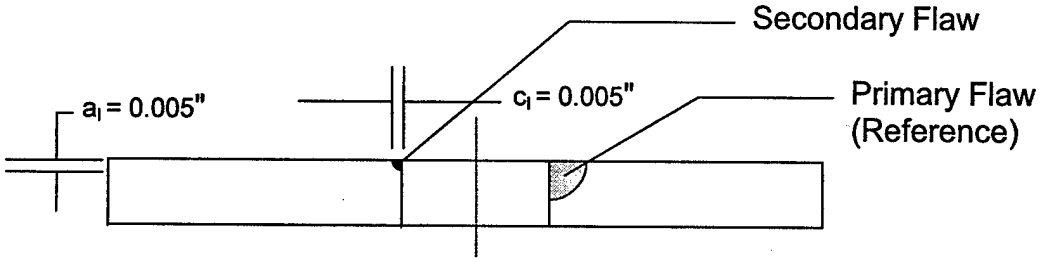


FIGURE 34. SECONDARY FLAW SIZE ASSUMPTIONS

## 3.3 DETERMINE INSPECTABLE FLAW SIZES FOR EACH CRITICAL LOCATION.

The detectable crack length and the probability of detection for the inspection program are affected by a number of factors. These factors include human factors, inspection method, instrument calibration procedure, structural geometry, and the degree of access. The objective is to define an inspection method that ensures a small detectable crack length will be discovered with a 90 percent probability of detection and a 95 percent confidence level. It is recommended that a nondestructive inspection technician that is certified to a minimum of a Level II in the applicable inspection method, as defined by the American Society for Nondestructive Testing Recommended Practice, Number SNT-TC-1A, be required for performing these inspections.

Eddy current and magnetic particle are the two inspection methods that were evaluated. The eddy-current inspection method is the recommended method for the majority of the critical areas due to its high sensitivity to fatigue cracks and a high probability of detection. The eddy-current method allows for a clean, relatively fast inspection without the use of chemicals, couplants, or paint stripping materials commonly used with other methods. Bolt hole and pencil probe surface eddy current are the two techniques applied to inspect for fatigue cracks on the Model 402 through "B" SID program. The magnetic particle inspection method is the recommended method for the inspection of the main landing gear side brace actuator collar due to its high fatigue crack sensitivity in ferromagnetic materials. Specific details about the required inspection method for each inspection location can be found in reference 4.

Bolt hole eddy current was chosen as the main inspection method for the Model 402 through "B" SID program for multiple reasons. Those reasons include the smallest detectable crack length, the ability to inspect at the crack origin, a high probability of detection, and a relatively low degree of inspection complexity. The minimum detectable crack length for bolt hole eddy current is 0.080 inch which is based upon the size of the calibration notch, the hole condition and the calibration method. This length will give the technician a large, easily distinguishable crack indication that will not be masked by holes that are slightly out of round. This technique was used for nearly all of the inspection areas, with the exception of the engine beam and landing gear areas.

The surface eddy-current technique is a simple and effective inspection technique for detecting fatigue cracks that are open to the surface or very near the surface. The main advantage of surface eddy current is that it applies the inspection coil directly to the inspection area without fastener removal. The detectable crack length for the surface eddy is calculated using the following equation:

$$\frac{\text{Fastener Head Diameter} - \text{Fastener Shank Diameter}}{2} + \text{Coil Diameter}$$

This formula accounts for the crack length that is hidden underneath the fastener head, which is not inspectable using this inspection technique. Surface eddy current will be the recommended technique for the engine beam area.

The magnetic particle inspection method is an effective inspection method due to its high sensitivity to surface and near surface fatigue cracks in ferromagnetic materials. The material for the 402 main landing gear side brace actuator collar is 4340 steel which lends itself to magnetic particle inspection. The combination of the magnetic field strength and the light intensity requirements allow a Level II magnetic particle inspection technician to inspect the critical areas with a detectable crack length of 0.050 inch.

## 3.4 PERFORM CRACK GROWTH ANALYSIS FOR EACH CRITICAL AREA.

A damage tolerance assessment (crack growth analysis) was conducted for both the Model 402C and the Model 402 through "B" airframe structures. The following steps were taken to conduct the damage tolerance assessment:

a. The analysis locations were identified, i.e., the critical areas of the PSE's as discussed in section 2.1 of this report.

b. The period of time required for a flaw to grow to a critical length was predicted.

c. The inspection intervals were determined, based on crack growth analysis and fail-safe capabilities, to maintain structural safety.

The analysis locations are presented in section 2.2.4 of this report. The details of each analysis are presented in appendix C of reference 3. The methodology used to calculate crack growth is presented in section 3.4.1. The results of the damage tolerance analysis are summarized in the form of crack growth curves. An example of a crack growth curve with and without the effects of retardation is shown in figure 35. Crack growth curves were generated for the Model 402C using three flight profiles: the Typical Flight Spectrum, the Severe Flight Spectrum, and the Short Flight Spectrum. Crack growth curves were generated for the Model 402 through "B" using two flight profiles: the Typical Flight Spectrum and the Severe Flight Spectrum. The crack growth curves for each of the analysis locations are presented in appendix C of reference 3.

The inspection intervals required to maintain structural safety are discussed in section 3.5.

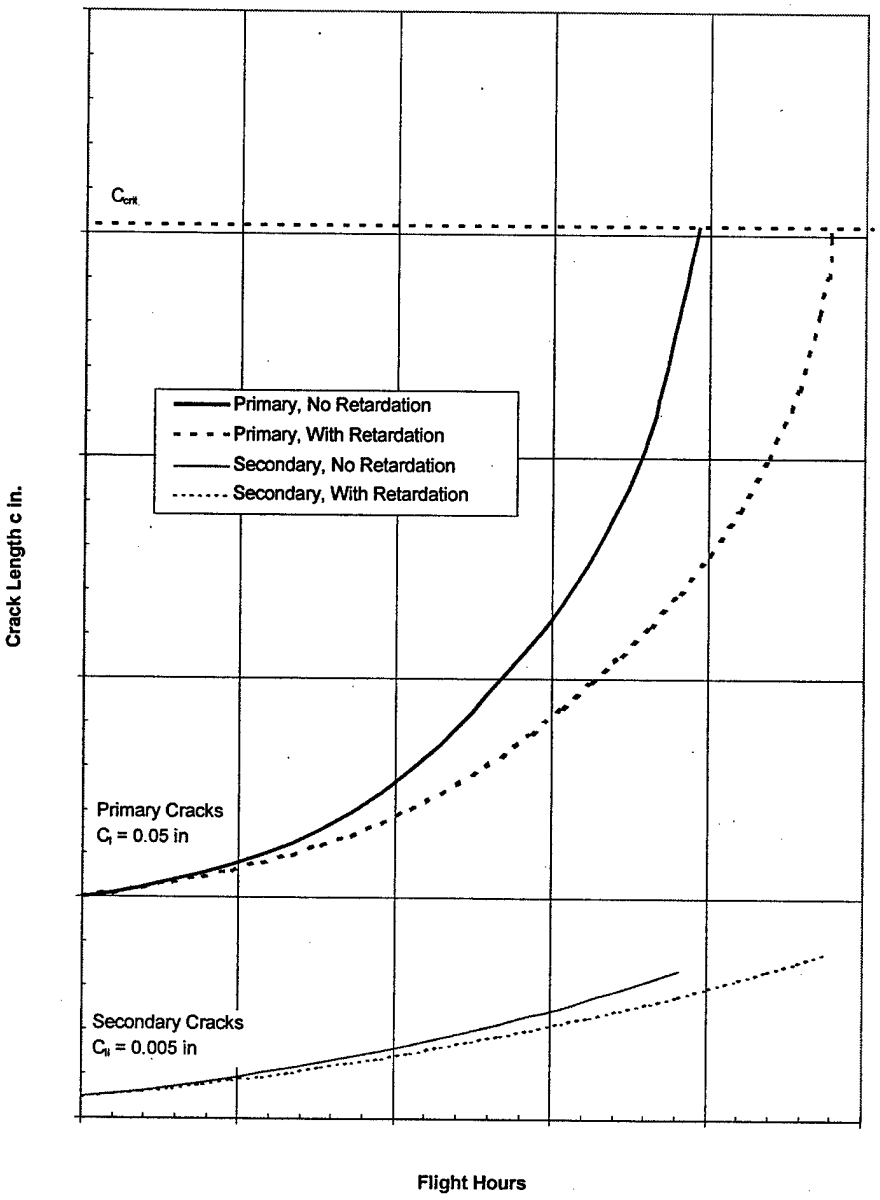


FIGURE 35. TYPICAL CRACK GROWTH CURVES WITH AND WITHOUT RETARDATION

3.4.1 Crack Growth Methodology.

Cracks were analytically propagated in a variable amplitude cyclic stress environment. A flight-by-flight loading is applied on a random cycle-by-cycle basis in the vicinity of the crack site. Crack growth is primarily a function of stress-intensity history and material properties. The rate of change of crack length, a, with a repeated application of load (N times) is defined by

$$\frac{da}{dN} = f(\Delta K, \text{Material})$$

where $\Delta K$, the stress-intensity solution, is a function of stress ($\sigma$), crack length, and a geometry factor (B) of the form

$$\Delta K = \Delta \sigma \sqrt{\pi a}\ B$$

The time for a crack to grow from an initial length ($a_i$) to a final length ($a_f$) is given by

$$N = \int_{a_i}^{a_f} \frac{1}{f(\Delta K, \text{Material})} da$$

The above integration can only be carried out numerically. The University of Dayton Research Institute's (UDRI) CRACKS95 [12] is used for crack growth life prediction. The CRACKS95 system is a crack growth life calculation algorithm which is based on the linear elastic fracture mechanics approach for estimating the fatigue life of a component with a crack.

Two different methods of determining the crack growth rate term were used depending upon the source of the material da/dN. Some of the da/dN data collected is the result of coupon testing done by Cessna in support of the durability and damage tolerance efforts. All other data were obtained from the NASA FLAGRO material database [13]. These two methods of determining da/dN are discussed in the following paragraphs.

The Walker-Chang equation of crack growth, used for Cessna generated material data, is

$$\frac{da}{dN} = C[(1-R_{eff})^m K_{max}^{eff}]^n \qquad R_{cut} > R > 0 \text{ and } \Delta K > \Delta K_{th}$$

$$\frac{da}{dN} = C[(1+R_{eff}^2)^q K_{max}^{eff}]^n \qquad R_{cutn} < R < 0 \text{ and } \Delta K > \Delta K_{th}$$

$$\frac{da}{dN} = 0 \qquad \Delta K < \Delta K_{th}$$

where:

$\frac{da}{dN}$ = crack growth rate

$R_{eff}$ = effective stress ratio

$K_{max}^{eff}$ = maximum stress-intensity factor

C,m,n = empirical constants

q = acceleration index

$R_{cut}$ - positive stress ratio cutoff limit, above which the material does not exhibit additional stress ratio effects

$R_{cutn}$ - negative stress ratio cutoff limit, below which the material does not exhibit additional stress ratio effects

The values of C, m, n, and q are obtained from the material data. For values of R that exceed $R_{cut}$, $R_{cut}$ is used instead. Also, there is no crack growth below the threshold value of $\Delta K$. The threshold is a function of R and material:

$$\Delta K_{th}(R) = \Delta K_{th}(0)\cdot(1-A_{th}\cdot R)$$

where: $\Delta K_{th}(0)$ = threshold stress-intensity factor at R=0
$\Delta K_{th}(R)$ = threshold stress-intensity factor at any stress ratio, R
$A_{th}$ = threshold modifier

for a positive stress ratio, $R > 0$. For negative stress ratio, $R<0$

$$\Delta K_{th}(R<0) = \Delta K_{th}(0)$$

The recommended values for the fracture threshold parameters $\Delta K_{th}$ (0) and $A_{th}$ are as follows:

| | |
|---|---|
| Aluminum | $\Delta K_{th}(0) = 2.38$, $A_{th} = 0.833$ |
| Steel | $\Delta K_{th}(0) = 2.75$, $A_{th} = 0.353$ [12] |

The NASGRO 2.0 equation of crack growth was used for the materials which originated from the NASA FLAGRO database, which is given by

$$\frac{da}{dN} = \frac{C(1-f)^n \Delta K^n (1-\frac{\Delta K_{th}}{\Delta K})^p}{(1-R)^n (1-\frac{\Delta K}{(1-R)K_c})^q}$$

where: $\frac{da}{dN}$ = crack growth rate
R = stress ratio
C,n,p,q = empirical constants
f = crack opening function
$\Delta K_{th}$ = threshold stress-intensity factor
$K_c$ = critical stress-intensity factor

The values of C, n, p, and q are obtained from the material data.

Load interaction was considered for those wing, horizontal stabilizer, and vertical stabilizer locations with relatively short lives. A load interaction model describes the effects of relatively large loads on the damage caused by subsequent smaller loads. Crack growth under variable-amplitude cycling is generally complicated by interaction between high and low loads. A high load occurring in a sequence of low-amplitude cycles significantly reduces the rate of crack-growth during the cycles applied subsequent to the overload. This phenomenon is called retardation.

The Willenborg-Chang load interaction model was used in the CRACKS95 program to more accurately model crack growth. In the Willenborg-Chang model, the overload interaction zone is reduced whenever the stress-intensity factor ratio is negative, and the current load is an overload condition. If the current load is not an overload or if the minimum stress-intensity factor due to an overload is greater than 0, the Willenborg-Chang model is the same as the generalized Willenborg model.

The residual stress-intensity factor $K_{red}$ used to calculate the effective stress-intensity factors $K_{max}^{eff}$ and $K_{min}^{eff}$ is accounted for in the generalized Willenborg retardation model in the form

$$K_{red} = \Phi\left[K_{max}^{OL}\sqrt{1-\frac{a-a_{OL}}{r_y^{OL}}}-K_{max}\right] >=0,$$

where: $\Phi$ = Proportionality Factor $= \dfrac{1-(\Delta K_{th_o}/K_{max})}{R_{so}-1}$

$K_{max}^{OL}$ = maximum stress-intensity factor of prior overload

$= \sigma_{max}^{OL}\sqrt{\pi a_{OL}}B_T$

$r_y^{OL}$ = plastic zone for prior overload

$= \dfrac{1}{2\pi}\left(\dfrac{K_{max}^{OL}}{F_{t_y}}\right)^2$ for plane stress or

$r_y^{OL} = \dfrac{1}{4\pi\sqrt{2}}\left(\dfrac{K_{max}^{OL}}{F_{t_y}}\right)^2$ for plane strain.

In the Willenborg-Chang model, the overload interaction zone is reduced whenever the stress-intensity factor ratio is negative and the current load is an overload condition. If $K_{min}^{OL}$ is less than zero, the extent of the plastic zone associated with the overload $K_{max}^{OL}$ is reduced

$$r_y^{OL} = 1+\left(\frac{K_{min}^{OL}}{K_{max}^{OL}}\right)^2 r_y^{OL}$$

where: $K_{max}^{OL}$ = maximum stress-intensity factor due to overload

$K_{min}^{OL}$ = minimum stress-intensity factor due to overload

If $K_{min}^{OL}/K_{max}^{OL}$ is less than $R_{cutn}$, the extent of the overload plastic zone is reduced by

$$r_y^{OL} = \left(1+R_{cutn}\right) r_y^{OL}$$

where: $R_{cutn}$ = negative stress ratio cutoff limit, below which the material does not exhibit additional stress ratio effects.

The effective stress-intensity factor for the overload ($K_{max}^{OL}$) - underload ($K_{min}^{OL}$) combination is

$$K_{max}^{OL} = F_{t_y}\sqrt{\alpha\pi r_y^{OL}}$$

where: $F_{t_y}$ = material yield strength

$\alpha = 2$ for plane stress

$\alpha = 4\sqrt{2}$ for plane strain.

There is no-load interaction due to the overload.

A Willenborg-Chang shut-off ratio ($R_{so}$) of 2.3 was used for 2000 series aluminum and a value of 2.65 was used for 7000 series aluminum. These values are considered to be conservative based on industry experience. These values were shown to be conservative by conducting spectrum loaded coupon tests for the most critical locations, using the typical flight spectrum. These tests are discussed in section 3.1.2.3.

Clipped spectra were generated for those wing, horizontal stabilizer, and vertical stabilizer locations which were analyzed with retardation effects. The clipping level was taken at the 1/10 flight level of the composite exceedance curve. The stress level at the 88 exceedances per 1000 flight hours (881 flights) was taken as the clipping level for the typical spectrum. The stress level at the 105 exceedances per 1000 flight hours (1048 flights) and 238 exceedances per 1000 flight hours (2381 flights) was taken as the clipping level for the Grand Canyon and Short Flight spectrums respectively. Maximum stresses above the maximum clipping level were changed to the maximum clipping level; likewise, minimum stresses below the minimum clipping levels were changed to the minimum clipping levels. The spectrums were cycle-counted using the range pair technique commonly referred to as the NLR method. The crack growth results can be found in appendix C of reference 3.

3.4.2 Stress-Intensity Factor Solution.

The crack growth of a part is related to the stress history on the part through the stress-intensity defined as

$$K = \sigma\sqrt{\pi c}\ B$$

where: $\sigma$ = gross area (far field) stress;

c = surface crack length for a single crack tip; and

B is a factor which accounts for the type of loading, the part geometry, and the shape of the crack. The stress-intensity (geometric) correction factor is 1.0 for a through-the-thickness crack in an infinitely wide plate, but for all other geometry,

$$B_T = \prod_{i=m}^{n} B_i$$

where: $B_i$ is the geometric correction factor for each specific deviation from a through crack in an infinite plate.

The most common solutions are pin loaded holes in a tension field (spar caps). For this solution, the two-dimensional corner crack model of Newman and Raju from the built-in CRACKS95 solutions library will be used. The CRACKS95 contains many other solutions.

3.4.3 Critical Crack Length and Residual Strength.

Fracture failure of a part or system of parts occurs when, due to the presence of a crack, the part no longer has sufficient residual strength to withstand application of additional load. In an unflawed structure, the residual strength is based on the allowable tensile strength ($F_{t_u}$) of the material. In a cracked structure, the residual strength is less than $F_{t_u}$ and decreases nonlinearly as the crack increases is size. Complete or partial failure of a part does not necessarily lead to failure of the aircraft nor even to total failure of the part itself (crack arrest).

Residual strength analysis can be used to solve either of the following problems:

a. Determine the load carrying capability of a structural member containing a crack of known length, or

b. Determine the critical crack length corresponding to a particular load level (limit load or max spectrum load).

The general stress-intensity formula can be used to determine the solution to either of these problems

$$\Delta K = \Delta \sigma \sqrt{\pi c}\ B$$

By rearranging the equation to the form

$$\sigma_{crit} = \frac{K_{crit}}{\sqrt{\pi c} B_T}$$

the critical stress ($\sigma_{crit}$) can be calculated for a known crack length, where:

$K_{crit}$ = Fracture Toughness ($K_c$ or $K_{1c}$),
$c$ = surface crack length for a single crack tip, and
$B_T$ = Geometric correction factor.

Rearranging the equation to the form

$$c_{crit} = \frac{1}{\pi}\left(\frac{K_{crit}}{\sigma_{crit} B_T}\right)^2$$

allows for the calculation of the limit load critical crack length ($c_{crit}$). However since $B_T$ is a function of c, it becomes iterative. It is more convenient to plot $\sigma_{crit}$ vs $c_{crit}$. This method permits incorporating upper boundary conditions for small cracks. For crack lengths approaching zero a boundary condition corresponding to 95% $F_{t_u}$ is chosen.

For most cases of crack growth (such as a cap, stringer, or other nonskin structure), failure is defined as the minimum of either net-section yielding or plane-strain toughness ($K_{1c}$). $K_{1c}$ is conservatively used instead of $K_c$ including those cases where a through-the-thickness crack could be considered as growing under plane-stress conditions. Figure 36 illustrates this concept. Critical crack lengths for each analysis location are documented in appendix C of reference 3.

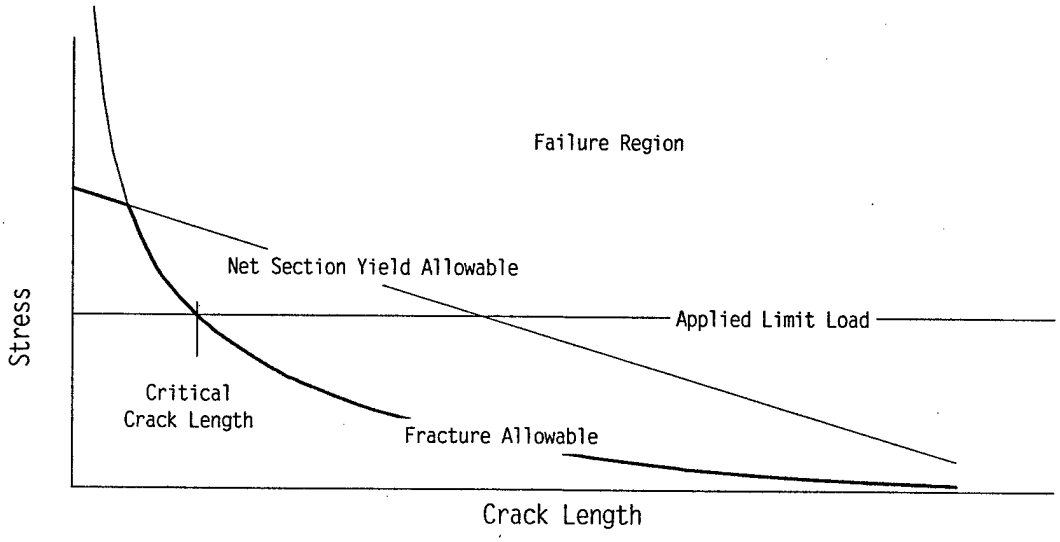


FIGURE 36. RESIDUAL STRENGTH ANALYSIS CRITERIA

## 3.5 ESTABLISH SUPPLEMENTAL INSPECTION THRESHOLD FOR EACH CRITICAL AREA.

### 3.5.1 Initial Inspections.

Initial inspections of a particular area of structure are based on both crack growth and fatigue analytical results. For structures which were proven to be fail-safe (see section 3.5.2) the initial inspections were based on fatigue life. For locations with long fatigue lives, the maximum initial inspection was limited to 15,000 flight hours. Structure which was proven to be fail-safe included the Model 402C wing, fuselage, and empennage and the Model 402 through "B" fuselage and empennage.

The Model 402 through "B" wing and engine beams and the Model 402C engine beams were not fail-safe tested. For these locations initial inspections of a particular area of structure were based on crack growth. For these locations, initial inspections are targeted for a point in time equal to one-half the time it takes for an initial flaw ($c_{init}$) to grow to a critical length ($c_{crit}$). The $c_{init}$ is generally assumed to be a 0.05-inch quarter-circular flaw for most structure and the $c_{crit}$ is the crack size beyond which the part can no longer take the maximum required load.

$$\text{Initial Inspection Time} = \frac{[\text{Flight Hours@}c_{critical} - \text{Flight Hours@}c_{initial}]}{2}$$

The initial inspections based on crack growth are shown graphically in figure 37. Recommended initial inspection times are given in the Model 402 SID [4].

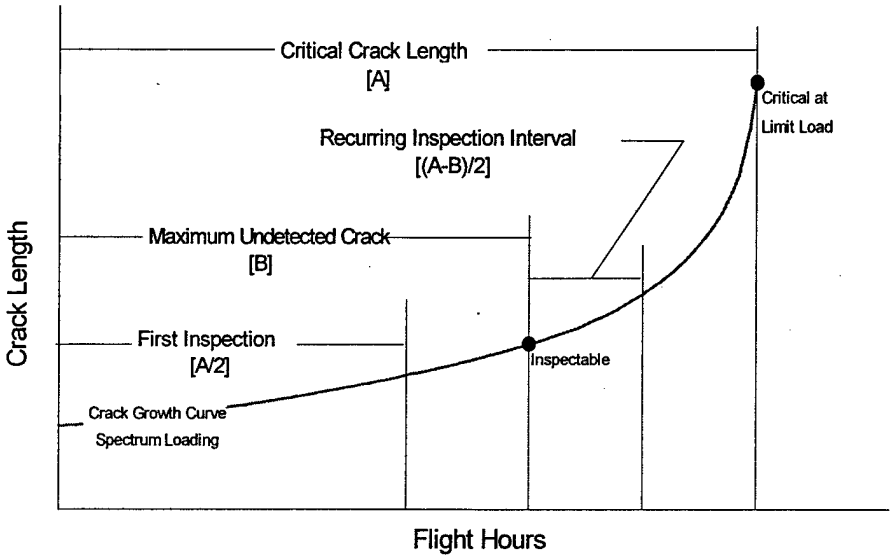


FIGURE 37. MULTIPLE LOAD PATH INSPECTION CRITERIA

3.5.2 Fail-Safe Tests.

Fail-safe tests were conducted to determine the fail-safe characteristics of the Model 402C wing and empennage. The results show compliance with the fail-safe requirements of FAR 23.572. The fail-safe test results demonstrate that catastrophic failure or excessive deformation which could adversely affect the aircraft flight characteristics will not occur after fatigue failure or obvious partial failure of a single principal structural element. The details of these tests are presented in the following paragraphs.

3.5.2.1 Empennage Fail-Safe Tests.

A series of fail-safe tests were conducted on the Model 402C empennage. Six fail-safe conditions, two vertical stabilizer and four horizontal stabilizer conditions, were tested. The selection of these test conditions was based on field experience as well as an extensive analytical

evaluation of the empennage structure. The empennage structure was evaluated in two steps. First, the internal loads output from the NASTRAN model of the empennage was reviewed to determine the critical components of the empennage for the critical loading conditions. Second, the NASTRAN model was run for the critical load case with the critical components failed in the model. The internal loads output from each failure was reviewed to determine which failures would be the most critical. If the NASTRAN model showed either a significant loss in margin of safety or a negative margin of safety with one of its elements removed then that location was chosen for testing.

The tests were conducted on an empennage (tailcone and horizontal and vertical stabilizers) obtained from a salvage yard. This is the same article used for the ground tests. Two types of fail-safe damage were used on the Model 402C empennage test article: (1) bolt removal and (2) saw cuts. When possible, bolts were removed to simulate damaged or failed members to preserve the test article as much as possible. The test article was returned to the original or equivalent strength by replacing the bolts and by structural repair of the saw cuts.

The empennage test article was loaded to a minimum of 86.25% of the critical limit load [75% of the critical limit load x 1.15 dynamic factor] to show compliance with the fail-safe requirements of FAR 23.572. The remaining structure supported the load without excessive deformation or failure for each of the six fail-safe conditions.

3.5.2.2 Wing Fail-Safe Tests.

A single fail-safe test was conducted on the Model 402C wing. The wing front spar lower cap was cut at WS 80.05. The selection of this test condition was based on an extensive analytical evaluation of the wing structure.

The wing structure was evaluated in two steps. First, the internal loads output from the NASTRAN model of the wing was reviewed to determine the critical components of the wing structure for the critical loading conditions. Second, the NASTRAN model was run for the critical load case with the critical components failed in the model. The internal loads output from each failure was reviewed to determine which failures would be the most critical. If the NASTRAN model showed either a significant loss in margin of safety or a negative margin of safety with one of its elements removed, then that location was chosen for testing. Four locations were considered for fail-safe testing. One fail-safe condition was tested, while the other three fail-safe conditions were evaluated analytically.

The fail-safe test was conducted on a left-hand wing obtained from a salvage yard, attached to a Model 425 fuselage. A Model 402C right-hand wing was obtained to use as a loading fixture. The Model 402C wing was fail-safe tested using one loading condition: maximum positive bending. The test condition covers the positive load envelope. The load envelope is a composite of the flight critical loads, based on requirements of CAR conditions 3.183 through 3.190. The test article was loaded to 86.25% of the critical limit load [75% of the critical limit load x 1.15 dynamic factor] to show compliance with the fail-safe requirements of FAR 23.572. The article was then loaded to 100% of the critical limit load. Strain gauge and deflection data were recorded during the test.

Fail-safe analyses were conducted for three wing locations in lieu of testing. An analysis was also conducted for location W-1 and compared to the fail-safe test results. The results show compliance to a minimum of 86.25% of the critical limit load [75% of the critical limit load x 1.15 dynamic factor] per the fail-safe requirements of FAR 23.572.

3.5.3 Fatigue Analysis.

Fatigue analyses were conducted for the Model 402 through "B" and Model 402C airframe locations shown in section 2.2.4. The fatigue analysis was conducted to give an indication of economic life of the airframe. The fatigue analysis results of the landing gear and the airframe structure proven to be fail-safe were used to determine initial inspection intervals.

Fatigue analyses are based on the Palmgren-Miner linear cumulative damage theory where the life limit is established when the summation of applied cycles divided by cycles to crack initiation equals one. These analyses incorporate the repeated loads spectra, stress equations, net area factors, and transfer factors defined for each analysis location. The stress endurance data used was based on cyclic test experience.

The S-N curves used for aluminum structure are based on previous full-scale and component fatigue test history at Cessna for similar structure and spectra. This method has advantages over methods where stress concentration factors are calculated and damage is cumulated through S-N curves based on $K_t$. The Cessna method will account for fretting and clamp-up that would be difficult using the $K_t$ approach.

The analytical mean life predicted by the analysis is defined as the time when 50% of the fleet aircraft are expected to have developed small cracks (typically 0.05 inch in length). The analytical mean life is based on a severity index, $K_f$. The severity index is representative of the specific geometric stress concentration for each location, the material condition, and previous cyclic test results of Cessna aircraft. For the Model 402, analyses were conducted for a range of $K_f$ values from 3.0 to 9.0. The S-N curves are graded according to their $K_f$ value from a mild 3.0 to a severe 9.0. The severity index was then selected based on cyclic test data. If cyclic test data were not available for the location, a $K_f$ value of 6.0 was selected. Selection of this $K_f$ factor is considered conservative compared with the actual derived $K_f$'s from other Cessna tests of similar structure.

The mean life was divided by a scatter factor. The scatter factor chosen is based on the guidelines of reference 6. For those locations with fatigue test data available a scatter factor of 4 was chosen. For those locations without test data, a scatter factor of 8 was chosen.

3.6 ESTABLISH REPEAT INSPECTION INTERVAL FOR EACH CRITICAL AREA.

Recurring inspections are performed after the initial inspection at intervals equal to one-half the time it takes for a crack to grow from the detectable length to the maximum allowable flaw size. This provides at least two chances to detect the crack before it grows to the maximum allowable flaw size.

The recurring inspection times are determined by:

a. Maximum undetectable flaw size—The maximum undetectable flaw size ($c_{insp}$) is unique for each location and is dependent on the method of inspection used.

b. Spectrum loaded crack growth—The crack growth is defined as a function of flight hours and is naturally unique for each location.

c. Maximum allowable flaw size—The maximum allowable flaw sizes ($c_{crit}$) are presented in section D.2 of reference 3.

The maximum allowable flaw size ($c_{crit}$) is the crack size beyond which the part can no longer take the maximum required load. There is no direct relationship between the maximum spectrum stress used to define the crack growth and the maximum (limit) load that the part is required to withstand. Figure 37 presents the inspection requirements for multiple load path structure. This approach defines the inspections for the majority of locations.

$$\text{Recurring Inspection Time} = \frac{[\text{Flight Hours@}c_{critical} - \text{Flight Hours@}c_{inspectable}]}{2}$$

Recommended recurring inspection times based on the crack growth analysis are presented in the Model 402 SID, reference 4.

## 3.7 DETERMINE THE ONSET OF WIDESPREAD FATIGUE DAMAGE.

Widespread fatigue damage (WFD) in a structure is characterized by the simultaneous presence of cracks at multiple structural details that are of sufficient size and density whereby the structure will no longer meet its damage tolerance requirement. Sources of WFD are multisite damage (MSD) and multielement damage (MED). MSD is characterized by the simultaneous presence of fatigue cracks in the same structural element that may coalesce leading to a loss of required residual strength. Figure 38 shows examples of MSD. MED is characterized by the simultaneous presence of fatigue cracks in similar adjacent structural elements. Figure 39 shows an example of multielement damage.

The Model 402 through "B" and the Model 402C wing structures were investigated for the potential of WFD. Figure 40 flowcharts the process used to evaluate WFD. This process used to evaluate WFD is based on evaluation guidelines presented in the final report of the Airworthiness Assurance Working Group (AAWG) Industry Committee on Widespread Fatigue Damage [14].

The evaluation was used to identify the potential areas for WFD and to update the current inspection requirements for specific WFD locations and modify the local structure as required.

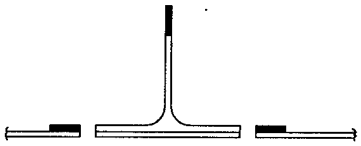

MSD in a Stringer

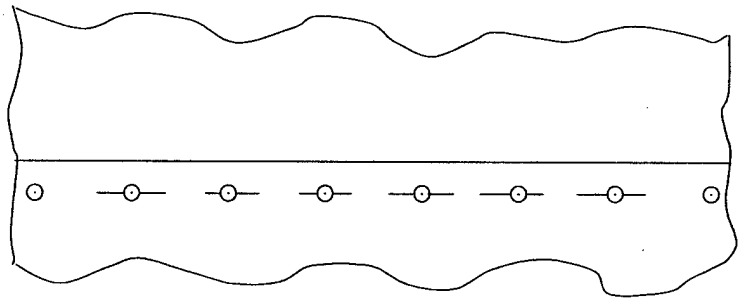

MSD at a Skin Splice

FIGURE 38. EXAMPLES OF MSD

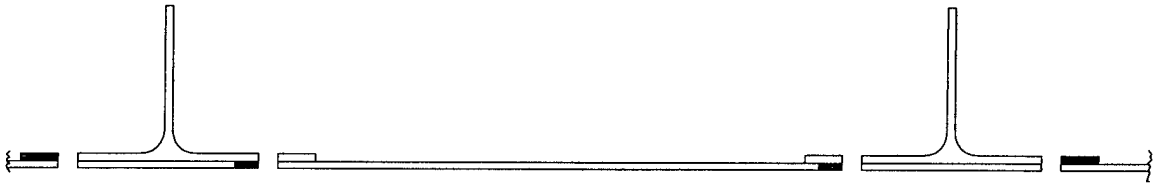

FIGURE 39. EXAMPLE OF MED

Sources of data used in the investigation of potential for WFD in the Model 402 through "B" wing included teardown evidence from full-scale and component cyclic test articles, FAA Service Difficulty Reports (FAA SDR's), Cessna Service Bulletins/Letters, and teardown evidence from high flight time field aircraft.

Sources of data used in the investigation of potential for WFD in the Model 402C wing include teardown evidence from full-scale cyclic test articles, FAA Service Difficulty Reports (FAA SDR's), and Cessna Service Bulletins/Letters.

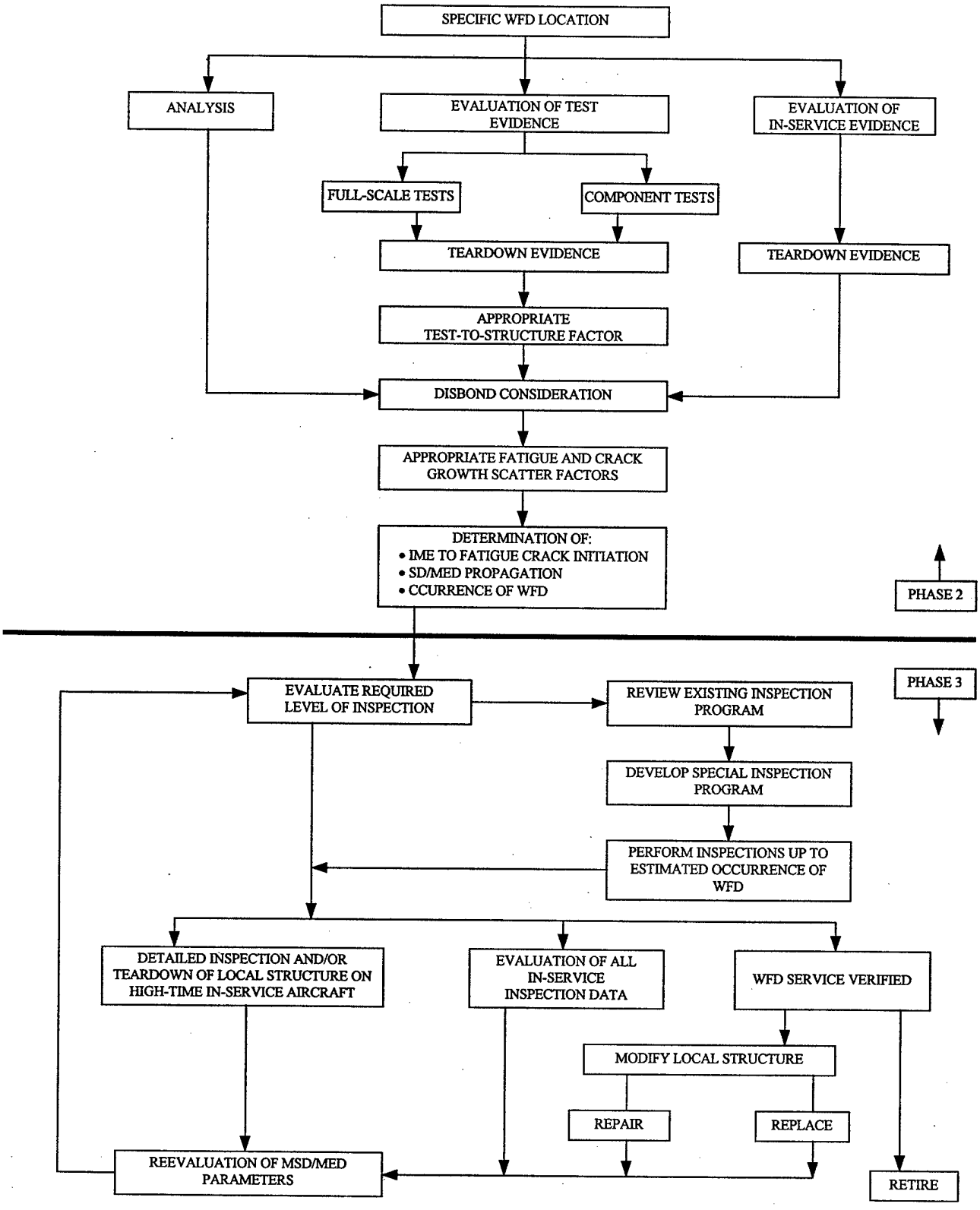


FIGURE 40. FLOWCHART OF WFD EVALUATION

## 4. PHASE 3 TASKS.

Phase 3 of the supplemental inspection document consisted of the following tasks:

a. Develop and analyze recommended design changes for the Model 402 through "B" and Model 402C wings.

b. Develop the Supplemental Inspection Document for the Cessna Model 402.

c. Develop the final report for the Model 402 SID program.

Results of the fatigue and damage tolerance analyses performed in Phase 2 indicated that modifications needed to be made to the Model 402 wing for the two main variations, the Model 402 through "B" and the Model 402C wings, to ensure continued airworthiness. The design changes that were developed for the Model 402 through "B" were analyzed in Phase 3. Interim Paper 2, reference 3, incorporates the results of the damage tolerance analyses conducted on the proposed modifications.

The design change analyzed for the Model 402 through "B" wing incorporated an external strap on the lower wing surface to reinforce the lower main spar cap of the wing. These changes are recommended for all aircraft with greater than 6500 hours flying in commercial operations. The modification analyzed for the Model 402C involves cold working the fastener holes attaching the skin to the lower main spar cap and installing oversized hi-lock fasteners. This change is recommended in order to reduce the number of repeat inspections which would otherwise be required as the planes age. These changes are recommended for all commercial aircraft with greater than 15,000 flight hours.

The Supplemental Inspection Document for the Cessna Model 402 was also developed in Phase 3. The SID for the Model 402 was developed by taking all inspections related to the Model 402 primary structure from the Cessna twin engine aircraft Continuing Airworthiness Program Document. Where necessary, the inspections were modified to reflect new inspection intervals determined in Phase 2 or to incorporate the latest state-of-the-art NDI inspection procedures. Also, since some new locations were analyzed in Phase 2, new inspections were developed for these locations for inclusion in the SID. The SID also incorporates the recommended modifications to the wing structure.

Lastly, the final report for the Model 402 SID program was developed in Phase 3. The final report (this document) is intended to summarize all activity performed during the development of the Cessna Model 402 SID.

## 5. CONCLUSIONS AND RECOMMENDATIONS.

- In order to assure the continued airworthiness of the commercially operated Model 402 fleet, strict compliance with the Model 402 SID is recommended, particularly for those airplanes operating in the severe flight or short flight regimes.

- The Model 402 through "B" and Model 402C wings are susceptible to fatigue. The inspection, structural repair, and structural modification requirements for the Model 402 through "B" and Model 402C wings, as detailed in the Model 402 SID [4], should be mandated for all commercially operated aircraft.

- In order for the Model 402 SID [4] to be successfully implemented, communication between all parties involved, the FAA, Cessna, and the Model 402 owner/operators, should be encouraged. Open communication will insure compliance with the Model 402 SID [4].

## 6. REFERENCES.


1. FAA Contract DTFA03-95-C-00044, Effective Date September 29, 1995.

2. Cessna Report S-402C-76-1, "M402 SID Interim Paper 1," June 25, 1996.

3. Cessna Report S-402C-76-2, "M402 SID Interim Paper 2," June 5, 1997.

4. Cessna Supplemental Inspection Document, Model 402.

5. FAA Report DOT/FAA/CT-91/20, "General Aviation Aircraft Normal Acceleration Data Analysis and Collection Project," February 1993.

6. FAA Report AFS-120-73-2, "Fatigue Evaluation of Wing and Associated Structure on Small Airplanes," May 1973.

7. "Progress Report on the NASA V-G/VGH General Aviation Program," National Aeronautics and Space Administration, SP-270, May 1971.

8. Engineering Science Data Item No. 69023 (Royal Aeronautical Society), "Average Gust Frequencies - Subsonic Transport Aircraft," with Amendments A and B, December 1970.

9. CAA letter, "Civil Aviation Authority Cessna Model 441 Conquest Evaluation Summary," April 2, 1976, 2nd Revision, May 2, 1977.

10. Cessna Report S-550-73, "Gear Load Survey," February 1984.

11. De Jonge, J. E., "The Monitoring of Fatigue Loads," National Luncht-en Ruimtevaart Laboratorium (NLR) MP 700104.

12. Gallagher, J.P., Miedlar, P.C., Cross, C.W., and Papp, M.L., "CRACKS95 System," University of Dayton Research Institute, Dayton, OH, November 1995.

13. Forman, R.G., "Fatigue Crack Growth Computer Program - NASA/FLAGRO," JSC-22267A, NASA/Lyndon B. Johnson Space Center, Houston, TX, August 1986, Revised March 1989.

14. Final Report of the Airworthiness Assurance Working Group - Industry Committee on Widespread Fatigue Damage, Mr. Ronald Wickens - Chairman, "Structural Fatigue Evaluation for Aging Airplanes," October 1993.

15. United States Air Force, AFGS-87221A, "General Specification for Aircraft Structures," June 8, 1990.

16. Department of Defense MIL-HDBK-5G, "Metallic Materials and Elements for Aerospace Vehicles Structures," November 1, 1994.

17. Gallagher, J.P., "A Compilation of Fracture and Crack Growth Data for High Strength Alloys," Damage Tolerance Design Handbook, MCIC-HB-01R, December 1983.

18. Editorial Staff, Reference Publications, American Society for Metals, "ASM Metals Reference Book," 2nd Edition 1983, American Society for Metals, Metals Park, Ohio 44073.

19. Chang, J. B. and Engle, R. M., "Improved Damage Tolerance Analysis Methodology," Journal of Aircraft Vol. 21, No. 9, p. 722.

20. ASTM E647-88a, "Standard Test Method for Measurement of Fatigue Crack Growth Rates," (American Society for Testing and Materials).

21. ASTM E561, "Standard Practice for R-Curve Determination" (American Society for Testing and Materials).